J|A|C|S
ARTICLES
Published on Web 06/20/2003

Functionalization of Single-Walled Carbon Nanotubes with (R-)Oxycarbonyl Nitrenes

Michael Holzinger,[†] Juergen Abraham,[†] Paul Whelan,[†] Ralf Graupner,[‡] Lothar Ley,[‡] Frank Hennrich,[§] Manfred Kappes,[§] and Andreas Hirsch*,[†]

Contribution from the Institut für Organische Chemie and Institut für Technische Physik, Friedrich-Alexander Universität Erlangen-Nürnberg, Henkestrasse 42, 91054 Erlangen, Germany, and Institut für Physikalische Chemie, Technische Universität Karlsruhe, Karlsruhe, Germany

Received December 27, 2002; E-mail: Hirsch@organik.uni-erlangen.de

Abstract: Sidewall functionalization of single-walled carbon nanotubes (SWCNTs) via the addition of (R-)-oxycarbonyl nitrenes allows for the covalent binding of a variety of different groups such as alkyl chains, aromatic groups, dendrimers, crown ethers, and oligoethylene glycol units. Such additions lead to a considerable increase in the solubility in organic solvents such as 1,1,2,2-tetrachloroethane (TCE), dimethyl sulfoxide (DMSO), and 1,2-dichlorobenzene (ODCB). The highest solubilities of 1.2 mg/mL were found for SWCNT adducts with nitrenes containing crown ether of oligoethylene glycol moieties in DMSO and TCE, respectively. The presence of chelating donor groups within the addends allowed for the complexation of Cu^{2+} and Cd^{2+}. Atomic force microscopy (AFM) and transmission electron microscopy (TEM) revealed that the functionalized tubes form thin bundles with typical diameters of 10 nm. The presence of thin bundles in solution is supported by ^1H NMR spectroscopy. The elemental composition of the functionalized SWCNT was determined by X-ray photoelectron spectroscopy (XPS). The use of Raman and electron absorption spectroscopy (UV/Vis−nIR) showed that the electronic properties of the SWCNTs are mostly retained after functionalization, indicating a low degree of addition within this series of SWCNT derivatives.

Introduction

Following the determination of the unique physical properties of single-walled carbon nanotubes (SWCNTs),[1−4] the question of possible technological applications quickly arose. On the way to technical applications, it was soon obvious that the tailoring of large ensembles of as pure and as uniform nanotubes as possible, rather than just single molecules, would be the major task. Presently the achievement of this goal represents a great challenge for chemists and material scientists. In this context, chemical functionalization[5,6] is an especially attractive target, since it can lead to increased solubility.[7] The establishment of nanotube chemistry will allow the combination of different materials with SWCNTs to create new compound classes with unprecedented properties and will form the basis for the processibility of these systems. A wide range of first approaches toward organic nanotube chemistry have been developed within the past few years. These include defect functionalization,[8−10] covalent functionalization of the sidewalls,[11−16] and noncovalent functionalization (for example, formation of supramolecular adducts with surfactants and polymers).[17−32]

[†] Institut für Organische Chemie, Universität Erlangen-Nürnberg.
[‡] Institut für Technische Physik, Universität Erlangen-Nürnberg.
[§] Institut für Physikalische Chemie, Universität Karlsruhe.

(1) Iijima, S. *Nature (London)* **1991**, *354*, 56.
(2) Rao, C. N. R.; Satishkumar, B. C.; Govindaraj, A.; Nath, M. *ChemPhysChem* **2001**, *2*, 78−105.
(3) Xie, S. S.; Chang, B. H.; Li, W. Z.; Pan, Z. W.; Sun, L. F.; Mao, J. M.; Chen, X. H.; Qian, L. X.; Zhou, W. Y. *Adv. Mater. (Weinheim, Germany)* **1999**, *11*, 1135−1138.
(4) Ajayan, P. M. *Chem. Rev. (Washington, D.C.)* **1999**, *99*, 1787−1799.
(5) Hirsch, A. *Angew. Chem., Int. Ed.* **2002**, *41*, 1853−1859.
(6) Bahr, J. L.; Tour, J. M. *J. Mater. Chem.* **2002**, *12*, 1952−1958.
(7) Bahr, J. L.; Mickelson, E. T.; Bronikowski, M. J.; Smalley, R. E.; Tour, J. M. *Chem. Commun. (Cambridge)* **2001**, 193−194.
(8) Chen, J.; Hamon, M. A.; Hu, H.; Chen, Y.; Rao, A. M.; Eklund, P. C.; Haddon, R. C. *Science (Washington, D. C.)* **1998**, *282*, 95−98.
(9) Haddon, R. C.; Chen, J. In *U.S.*; University of Kentucky Research Foundation; 2001; pp 8.
(10) Chen, J.; Rao, A. M.; Lyuksyutov, S.; Itkis, M. E.; Hamon, M. A.; Hu, H.; Cohn, R. W.; Eklund, P. C.; Colbert, D. T.; Smalley, R. E.; Haddon, R. C. *J. Phys. Chem. B* **2001**, *105*, 2525−2528.
(11) Mickelson, E. T.; Huffman, C. B.; Rinzler, A. G.; Smalley, R. E.; Hauge, R. H.; Margrave, J. L. *Chem. Phys. Lett.* **1998**, *296*, 188−194.
(12) Boul, P. J.; Liu, J.; Mickelson, E. T.; Huffman, C. B.; Ericson, L. M.; Chiang, I. W.; Smith, K. A.; Colbert, D. T.; Hauge, R. H.; Margrave, J. L.; Smalley, R. E. *Chem. Phys. Lett.* **1999**, *310*, 367−372.
(13) Bahr, J. L.; Yang, J.; Kosynkin, D. V.; Bronikowski, M. J.; Smalley, R. E.; Tour, J. M. *J. Am. Chem. Soc.* **2001**, *123*, 6536−6542.
(14) Holzinger, M.; Vostrowsky, O.; Hirsch, A.; Hennrich, F.; Kappes, M.; Weiss, R.; Jellen, F. *Angew. Chem., Int. Ed.* **2001**, *40*, 4002−4005.
(15) Georgakilas, V.; Kordatos, K.; Prato, M.; Guldi, D. M.; Holzinger, M.; Hirsch, A. *J. Am. Chem. Soc.* **2002**, *124*, 760.
(16) Georgakilas, V.; Voulgaris, D.; Vazquez, E.; Prato, M.; Guldi, D. M.; Kukovecz, A.; Kuzmany, H. *J Am. Chem. Soc.* **2002**, *124*, 14318−14319.
(17) Balavoine, F.; Schultz, P.; Richard, C.; Mallouh, V.; Ebbesen, T. W.; Mioskowski, C. *Angew. Chem., Int. Ed.* **1999**, *38*, 1912−1915.
(18) Chen, R. J.; Zhang, Y.; Wang, D.; Dai, H. *J. Am. Chem. Soc.* **2001**, *123*, 3838−3839.
(19) Coleman, J. N.; Dalton, A. B.; Curran, S.; Rubio, A.; Davey, A. P.; Drury, A.; McCarthy, B.; Lahr, B.; Ajayan, P. M.; Roth, S.; Barklie, R. C.; Blau, W. J. *Adv. Mater. (Weinheim, Germany)* **2000**, *12*, 213-216.
(20) O'Connell, M. J.; Boul, P.; Ericson, L. M.; Huffman, C.; Wang, Y.; Haroz, E.; Kuper, C.; Tour, J.; Ausman, K. D.; Smalley, R. E. *Chem. Phys. Lett.* **2001**, *342*, 265−271.
(21) Bandow, S.; Rao, A. M.; Williams, K. A.; Thess, A.; Smalley, R. E.; Eklund, P. C. *J. Phys. Chem. B* **1997**, *101*, 8839−8842.
(22) Duesberg, G. S.; Burghard, M.; Muster, J.; Philipp, G.; Roth, S. *Chem. Commun. (Cambridge)* **1998**, 435−436.

10.1021/ja029931w CCC: $25.00

Despite the steady progress in this area, it is important to mention that, in general, it is still very difficult to obtain unambiguous analytical data of functionalized SWCNTs allowing for a satisfying structure interpretation. This is related to the fact that the SWCNTs used as starting materials (a) aggregate as rather insoluble bundles of different diameters making a selective chemistry difficult, (b) vary greatly in length and diameter, and (c) possess a range of helicities and defects both at the tube ends and on the sidewalls.[5] Moreover, it is still very difficult to obtain SWCNTs that are free from impurities such as amorphous carbon and metal catalyst particles. As a consequence, all functionalized SWCNTs synthesized so far represent an extremely polydisperse mixture of compounds of, in most cases, undefined or difficult to define purity. Standard techniques for molecular structure characterization such as NMR spectroscopy or mass spectrometry are of limited use or cannot be applied. Therefore, there is a need for additional and, for synthetic chemists, less common techniques such as scanning probe microscopy.

Recently, we communicated on the covalent functionalization of SWCNTs with reactive species such as nitrenes, carbenes, and radicals.[14] Here we present a detailed study of nanotube chemistry using the reaction of SWCNTs with a broad range of (R-)oxycarbonyl nitrenes generated from the corresponding azidocarbonates. A detailed characterization of the reaction products using a variety of techniques is provided. XPS investigations were introduced for the analysis of functionalized SWCNTs. It was our intention to critically evaluate the scope and limitation of this type of covalent SWCNT chemistry, with particular emphasis on the conclusions that can validly be drawn from the compound characterization.

Results and Discussion

Synthesis of (R-)Oxycarbonyl-Functionalized SCWNTs. The SWCNTs used for this work were prepared by the laser ablation of graphite with 1% each of Co and Ni, as catalysts. The crude SWCNT soot was refluxed for 48 h in 2−3 M HNO_3, and the ultracentrifuged solid was resuspended in a 0.2 wt % Triton X-100 aqueous solution. The suspension was filtered through a 0.2 μm filter to give SWCNTs of 99% purity by weight as determined by oxidative thermogravimetric analysis (TGA).[33] These purified SWCNTs were used as the starting material for the functionalization process. The SWCNTs typically show a diameter distribution between about 1.2 and 1.4 nm. Further characterization of the SWCNT starting material is shown later in this work in comparison to the functionalized material.

The functionalization of SWCNTs with (R-)oxycarbonyl nitrenes is shown in Scheme 1. The synthesis of the azidocarbonates **3a** and **3b** was described previously.[34] The synthetic sequence leading to the new azidocarbonates **3c**−**n** started by the treatment of a commercially available alcohol with phosgene to form a chlorocarbonate.[35] For the synthesis of the chlorocarbonates (**2c**−**n**), a solution of the corresponding alcohol (**1c**−**n**) in toluene was added dropwise to a commercially available solution of 20 wt % phosgene in toluene at 0 °C. After 1 h, the reaction mixture was allowed to reach room temperature. The mixture was stirred at room temperature until TLC showed the complete conversion of the alcohol. In most cases, this was achieved after 10 h of stirring at room temperature. In some cases, however, stirring at 50 °C for another 4 h was necessary to complete the reaction. For the workup of the crude product, the excess of phosgene was removed with a nitrogen stream. After evaporation of the solvent, the highly pure choridocarbonates (**2c**−**n**) were obtained in almost quantitative yields. Complete characterization was carried out by ^{1}H NMR, ^{13}C NMR, MS, and IR spectroscopy. For the synthesis of the azidocarbonates (**3c**−**n**), the corresponding chlorocarbonates (**2c**−**n**) were dissolved in THF. After the addition of 1.5 equiv of sodium azide and a catalytic amount of 18-crown-6, the solution was stirred at room temperature. The progress of the reaction was monitored by IR spectroscopy, following the consumption of the chlorocarbonate by the disappearance of the CO−Cl band at 682−690 cm^{-1}. After the filtration of the sodium chloride precipitate, the solvent was evaporated to give the crude products. Further purification was carried out by column chromatography. For the final sidewall functionalization, the SWCNTs were dispersed in 1,2-dichlorobenzene (ODCB) in an ultrasonic bath under nitrogen atmosphere for several hours. The dark but still transparent solution was heated to 160 °C. At this temperature, a 200 wt % excess of azidocarbonate (**3a**−**n**), diluted with the solvent, was added dropwise over 20 min. After thermally induced N_2 extrusion, nitrene addition resulted in the formation of alkoxycarbonylaziridino-SWCNTs (**4a**−**n**). The reaction mixture was kept at this temperature for another 30 min and then allowed to cool to room temperature. Workup proceeded by separating the suspension of the derivatized SWCNTs (**4a**−**n**) from the insoluble contaminants, such as unmodified or barely modified SWCNTs, by decantation. The supernatant was diluted with a solvent such as acetone to induce flocculation of all dissolved SWCNTs. Subsequent centrifugation and washing of the residue results in the removal of soluble byproducts. The derivatized SWCNTs (**4a**−**n**) were dried under high vacuum (Scheme 1).The use of azidocarbonates is necessary for this type of reaction because alkyl azides would give rise to a [3 + 2]-cycloaddition prior to the N_2 extrusion. We attempted this type of reaction, but all experiments using alkyl azides as 1,3-dipoles in order to form [3 + 2]-adducts were unsuccessful.

Metal Complexation of SWCNT Derivatives 4j and 4k. The oligoether groups within the SWCNT derivatives **4j** and

(23) Krstic, V.; Duesberg, G. S.; Muster, J.; Burghard, M.; Roth, S. *Chem. Mater.* **1998**, *10*, 2338−2340.
(24) Tsang, S. C.; Davis, J. J.; Green, M. L. H.; Hill, H. A. O.; Leung, Y. C.; Sadler, P. J. *J. Chem. Soc., Chem. Commun.* **1995**, 2579.
(25) Tsang, S. C.; Guo, Z.; Chen, Y. K.; Green, M. L. H.; Hill, H. A. O.; Hambley, T. W.; Sadler, P. J. *Angew. Chem., Int. Ed. Engl.* **1997**, *36*, 2198−2200.
(26) Erlanger, B. F.; Chen, B.-X.; Zhu, M.; Brus, L. *Nano Lett.* **2001**, *1*, 465.
(27) Sun, Y.; Wilson, S. R.; Schuster, D. I. *J. Am. Chem. Soc.* **2001**, *123*, 5348.
(28) Kong, J.; Dai, H. *J. Phys. Chem. B* **2001**, *105*, 2890−2893.
(29) Curran, S. A.; Ajayan, P. M.; Blau, W. J.; Carroll, D. L.; Coleman, J. N.; Dalton, A. B.; Davey, A. P.; Drury, A.; McCarthy, B.; Maier, S.; Strevens, A. *Adv. Mater. (Weinheim, Germany)* **1998**, *10*, 1091−1093.
(30) Star, A.; Stoddart, J. F.; Steuerman, D.; Diehl, M.; Boukai, A.; Wong, E. W.; Yang, X.; Chung, S.-W.; Choi, H.; Heath, J. R. *Angew. Chem., Int. Ed.* **2001**, *40*, 1721−1725.
(31) Coleman, J. N.; Dalton, A. B.; Curran, S.; Rubio, A.; Davey, A. P.; Drury, A.; McCarthy, B.; Lahr, B.; Ajayan, P. M.; Roth, S.; Barklie, R. C.; Blau, W. J. *Adv. Mater. (Weinheim, Germany)* **2000**, *12*, 213-216.
(32) Star, A.; Steuerman, D. W.; Heath, J. R.; Stoddart, J. F. *Angew. Chem., Int. Ed.* **2002**, *41*, 2508−2512.
(33) Hennrich, F.; Lebedkin, S.; Malik, S.; Tracy, J.; Barczewski, M.; Roesner, H.; Kappes, M. *Phys. Chem. Chem. Phys.* **2002**, *4*, 2273−2277.
(34) Bodansky, M.; Bodansky, A. *The Practice of Peptide Synthesis*, 2 ed.; Springer-Verlag: Stuttgart, 1994.
(35) Matzner, M.; Kurkjy, R. P.; Cotter, R. J. *The Chemistry of Chloroformates*; Union Carbide Corp.: New Jersey, 1964.

Scheme 1. Sidewall Funtionalization of SWCNTs with Azidocarbonates[a]

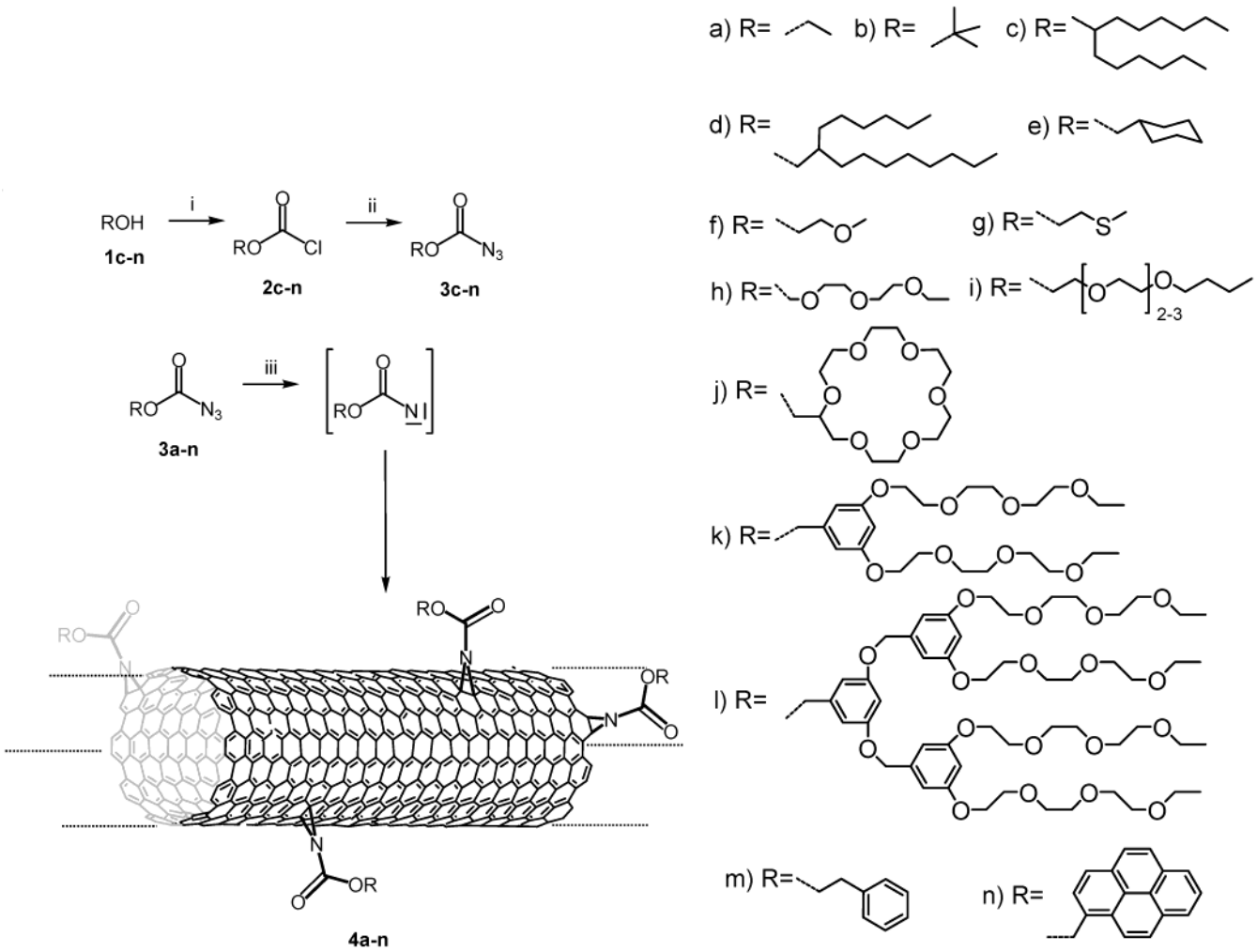

[a] (i) 20% phosgene in toluene, 0 °C to rt, 24 h; (ii) THF, rt, 18-crown-6, NaN_3, 4d; (iii) SWCNTs, ODCB, 160 °C, 1.5 h.

4k are capable of forming metal complexes. We therefore decided to carry out some complexation experiments, to investigate if these SWCNT derivatives maintain the complexation properties of the addends. We chose Cd and Cu as central metals for the complexation.

For this purpose we prepared a suspension of the corresponding SWCNT derivatives **4j** and **4k** and added a solution of the metal salt (Scheme 2). After a sonication period, the excess metal salt was removed by filtration through a 0.2 μm cellulose nitrate pore filter to form a "bucky paper", which was washed with distilled water. The resulting "bucky papers" **5j** and **5k** were dried under high vacuum.

Characterization of the Functionalized SWCNTs 4a−n. X-ray Photoelectron Spectroscopy (XPS). XPS turned out to be a powerful tool for the investigation of functionalized SWCNTs. As one can see in Figure 1, the spectrum of the SWCNT starting material shows the predominant presence of carbon (87 at. %) and oxygen (10 at. %). Minor amounts of nitrogen and iron are remnants from the purification process.

The XPS survey spectrum of **5j** (Figure S1) shows the presence of all expected elements associated with the compound. Small quantities of sodium and calcium were introduced, probably due to the washing with water. The atomic composition reveals an increase of oxygen, attributed to the oxygen atoms

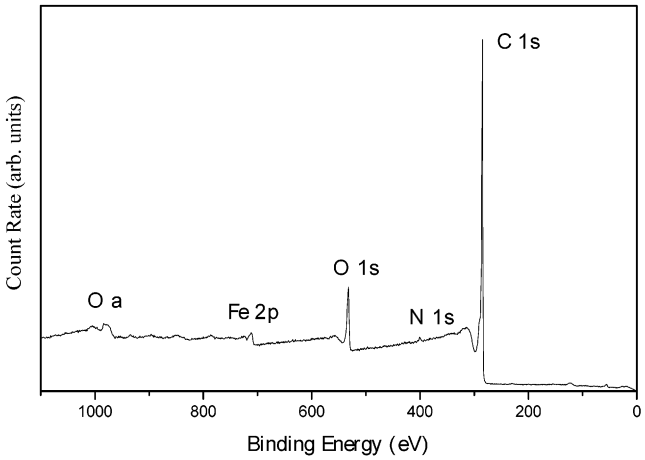

Figure 1. XPS survey spectrum of laser ablation SWCNTs purified by microfiltration. Composition: 87% C, 10% O, 1.3% N, 0.93% Fe.

in the crown ether addend of the SWCNT derivative **4j**. Moreover, the nitrogen in the aziridino group is reflected in the higher nitrogen content. The appearance of sulfur in the spectrum is introduced by sulfate, which might act as a counterion of the coordinated Cd^{2+}.

The C 1s spectrum of **5j** is displayed in Figure 2. This spectrum clearly consists of at least three components. The broad

Scheme 2. (a) Complexation of Cd^{2+} with **4j** and (b) Complexation of Cu^{2+} with **4k**

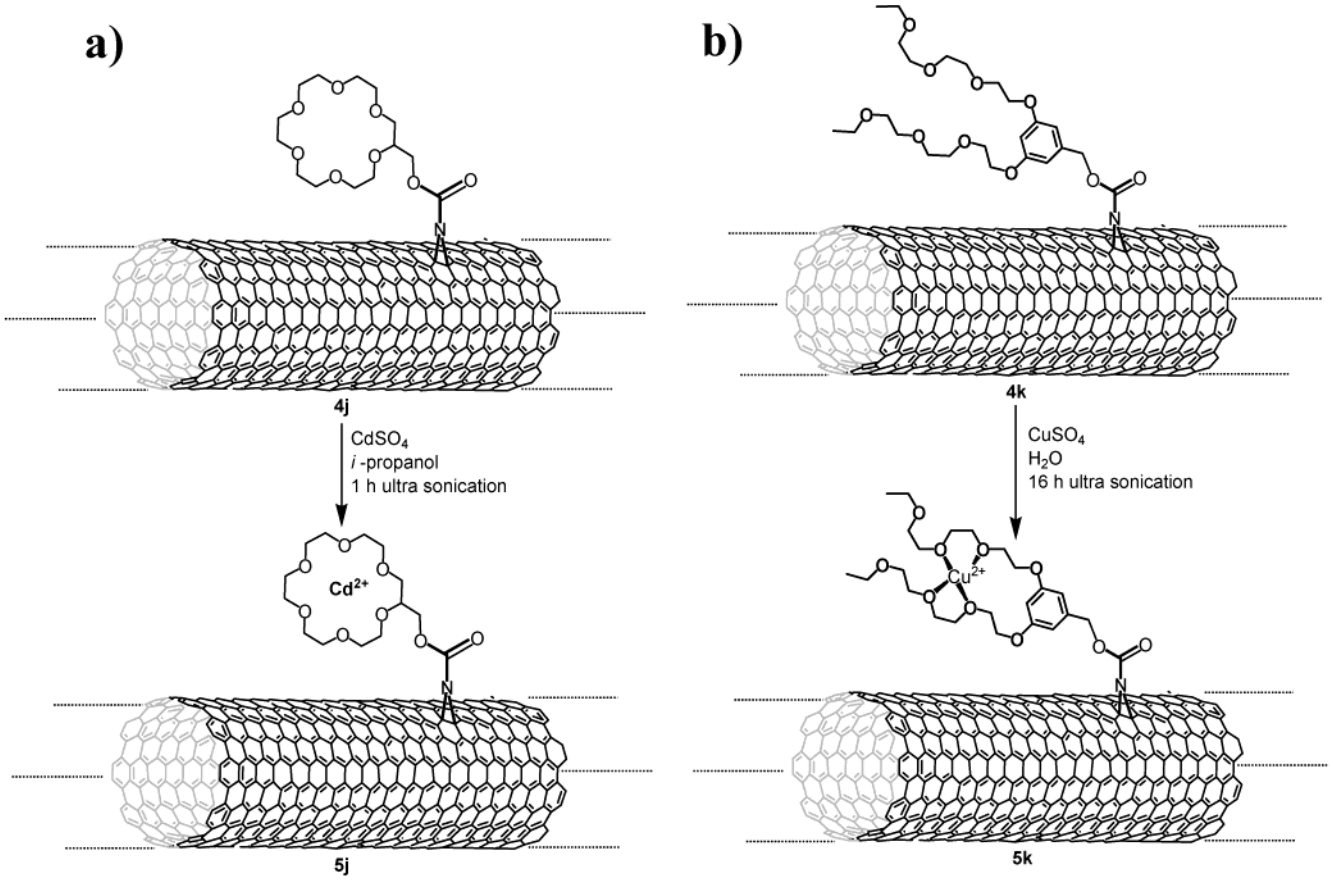

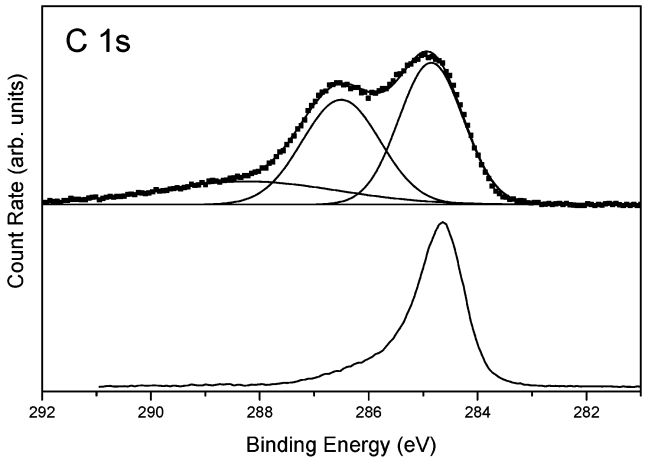

Figure 2. XPS C 1s spectrum of **5j** (upper spectrum) and SWCNT starting material (lower spectrum).

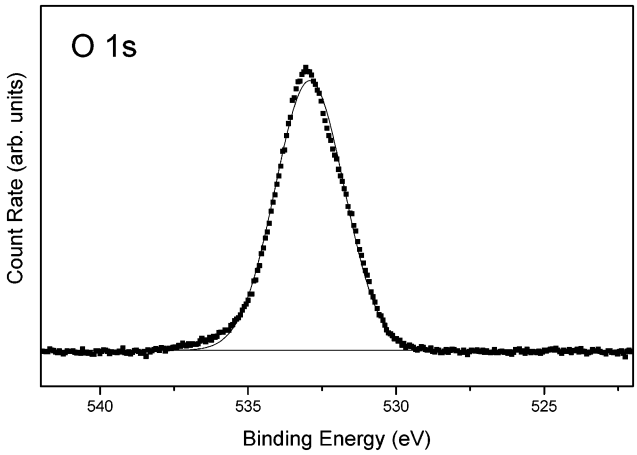

Figure 3. XPS O 1s spectrum of **5j**.

signal at 288 eV originates from carbon atoms bound to two oxygen atoms, such as carboxylic groups, from both the mildly oxidized SWCNTs and the addend.[36,37] The peak at 286.5 eV is due to emission from carbon atoms bound to one oxygen atom, i.e., the carbon atoms from the ether moiety. The measured peak position is consistent with XPS measurements of poly(propylene glycol) (PPG), where a peak at a binding energy of 286.44 eV is attributed to the carbon atoms bound to one oxygen atom.[38] The peak at 285 eV is due to the graphite-like carbon atoms of the tube walls.

The oxygen 1s core level of **5j**, shown in Figure 3, is located at 532.9 eV. This binding energy is slightly higher than that measured on PPG (532.7 eV). However, this difference in the position might arise due to various bonding environments of oxygen, other than the ether bonds, which are evident from the broad component at 288 eV in the C 1s spectrum (Figure 3).

In Figure S2, the N 1s and the Cd 3d core levels of **5j** are depicted. The measured binding energy of the Cd 3d 5/2 core level (406.0 eV) is indeed close to the binding energy measured

(36) Hamon, M. A.; Hu, H.; Bhowmik, P.; Niyogi, S.; Zhao, B.; Itkis, M. E.; Haddon, R. C. *Chem. Phys. Lett.* **2001**, *347*, 8−12.
(37) Mawhinney, D. B.; Naumenko, V.; Kuznetsova, A.; Yates, J. T.; Liu, J.; Smalley, R. E. *Chem. Phys. Lett.* **2000**, *324*, 213-216.
(38) Beamson, G.; Briggs, D. *High-Resolution XPS of Organic Polymers;* Ellis Harwood: Chichester, 1992.

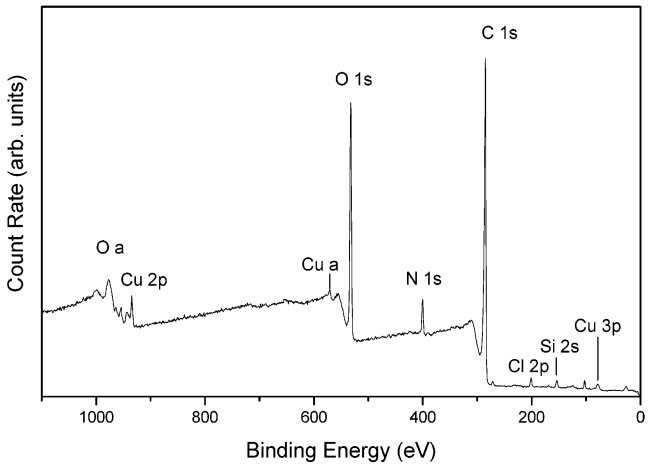

Figure 4. XPS survey spectrum of **5k**. Composition: 69.1% C, 1.4% Si, 0.7% Cl, 4.4% N, 23% O, 1.4% Cu.

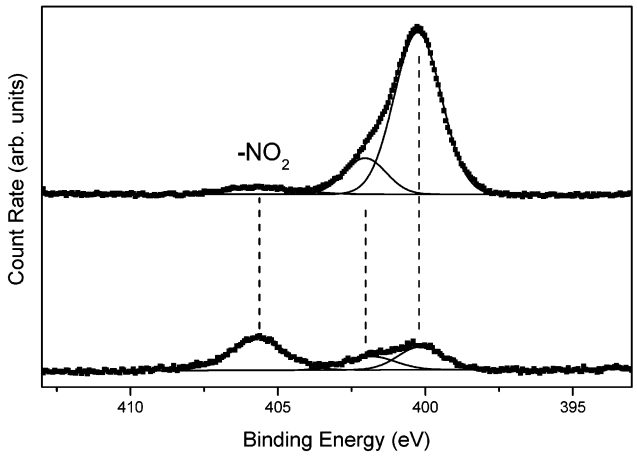

Figure 5. XPS N 1s spectrum of **5k** (top) and N 1s spectrum of the purified SWCNT starting material.

for related Cd^{2+} complexes (405.7 eV).[39] An additional contribution of nitrogen in NO_2 groups would also appear at 406 eV binding energy (see Figure 7). However, this contribution is negligible as the measured intensity ratio of the Cd spin−orbit splitted components (3d 5/2 to 3d 3/2) is 1.54, which is close to the expected ratio of the respective multiplicities (1.5). We therefore conclude from the ratio of the N to Cd content as well as from the Cd 3d core level positions that a significant rate of the crown ether addend of **5j** hosts Cd^{2+} ions.

The XPS survey spectrum of **5j** is shown in Figure 4. Again, all expected elements can be identified by their core levels. In addition, small amounts of silicon and chlorine can be detected. Both elements are often found to be present as impurities in our samples. The amount of nitrogen is also higher compared to the SWCNT starting material and is therefore attributed to the presence of the nitrogen-containing addend. In addition, the XPS spectrum shows clearly the presence of copper. Figure 5 shows the N 1s core level spectrum of **5k** compared to the N 1s spectrum of the purified SWCNT precursor.

A small peak is observed in the pristine material at around 406 eV. We attribute this peak to NO_2 groups, in agreement with measurements of poly(4-nitrostyrene) (PNS)[38] and nitrogen-containing carbonaceous materials.[40,41] The amount of NO_2 groups that were introduced by the purification process has clearly decreased in the spectrum of the functionalized SWCNTs compared to the SWCNT starting material; this indicates that NO_2 groups are split off during the functionalization process at 160 °C. However, the component at 400.3 eV shows a drastic increase. This component is related to nitrogen bound only to carbon atoms as nearest neighbors. We attribute it to the nitrogen atom within the aziridine groups. The origin of the small component at 402 eV is not yet clear.

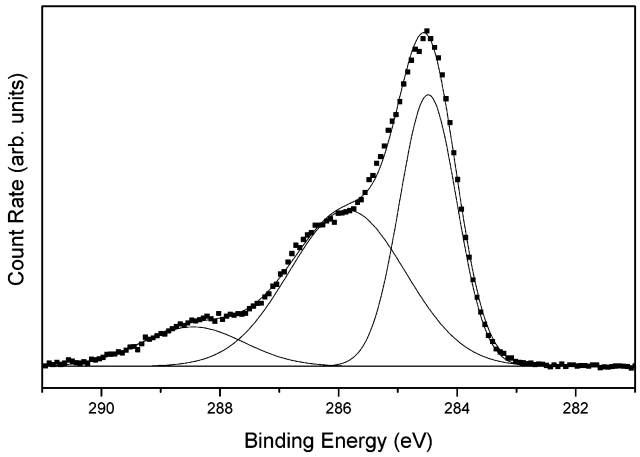

Figure 6. XPS C 1s spectrum of **5k**.

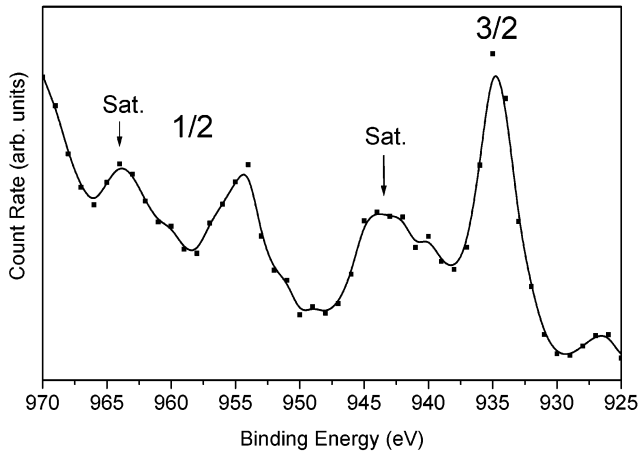

Figure 7. XPS Cu 2p core level spectra of sample **5k**.

The carbon core level spectrum of **5k** (Figure 6) shows a large number of carbon atoms bearing one oxygen atom. These atoms are assigned to the polyether groups of the addend. An increase in the number of carboxylic carbon atoms can also be detected that originates from the attached carbonates. These results correspond well with the data determined for **5j** (Figure 2). In Figure 9 the Cu 2p core levels of **5k** are shown.

The spectrum shows that the 2p 1/2 and 2p 3/2 lines are accompanied by satellite lines at 940−945 and 960−965 eV. It is known, that these satellite lines are characteristic for copper in the oxidation state of +2.[42] Identical satellites were found in other Cu(II) complexes.[43,44] The reason for the appearance of

(39) Adam, S.; Bauer, A.; Timpe, O.; Wild, U.; Mestl, G.; Bensch, W.; Schlogl, R. *Chem. Eur. J.* **1998**, *4*, 1458−1469.
(40) Pels, J. R.; Kapteijn, F.; Moulijin, J. A.; Zhu, Q.; Thomas, K. M. *Carbon* **1995**, *33*, 1641−1653.
(41) Pakula, M.; Biniak, S.; Swiatkowski, A.; Neffe, S. *Carbon* **2002**, *40*, 1873−1881.
(42) Van der Laan, G.; Westra, C.; Haas, C.; Sawatzky, G. A. *Phys. Rev. B: Condens. Matter* **1981**, *23*, 4369−4380.
(43) Okada, K.; Kawai, J.; Kotani, A. *Phys. Rev. B: Condens. Matter Mater. Phys.* **1993**, *48*, 10733−10738.

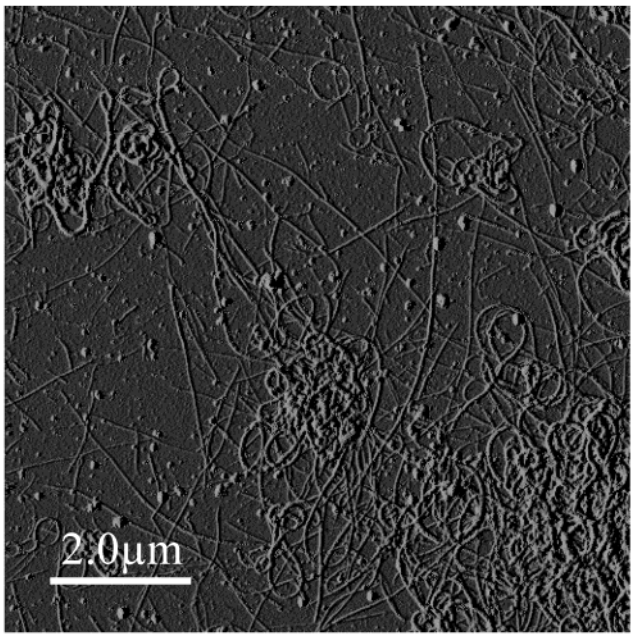

Figure 8. AFM image of purified SWCNT starting material.

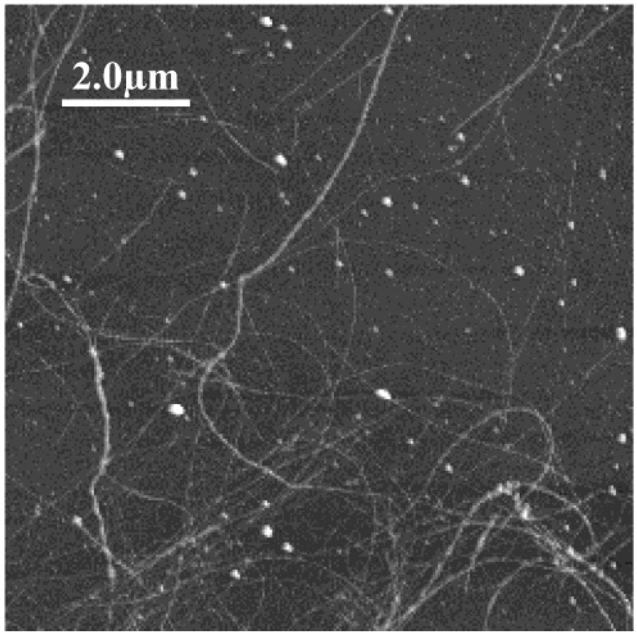

Figure 9. AFM image of **4b**.

several components in the core level spectra of Cu(II) compounds is the unfilled Cu 3d ($3d^9$) level in the Cu(II) state, which enables a charge transfer from the ligand to the copper atom, leading to different final states in the photoemission process. It is generally accepted that the main line corresponds to the "well screened" $2p^53d^{10}L$ state (L denotes the hole at the ligand). Whereas, the satellite corresponds to the "poorly screened" $2p^53d^9L$ state.[45] It is evident from the intensity of the satellite emission in Figure 7 (top) that the copper in sample **5k** is predominantly in the oxidation state of +2.

Furthermore the XPS data enabled us to give an estimate of the degree of functionalization via the comparison of the amount of nitrogen and carbon in the sample. This, however, presumes that all carbon atoms constitute to the tube sidewalls, whereas the nitrogen atoms are all part of the addend. The average degree of functionalization determined that way is less than 2% addend per C-atoms of the tube sidewalls (at. %) (Table 1). The limitations of the determination of the degree of functionalization are evident for the derivatives with more space filling addends, such as **4i**−**l,** where the evaluation of the XPS data gave values from 6 to 8 at. %. A closer look on the C1s core level reveals that, due to limitations caused by the inelastic mean free path of the photoelectrons (~5 Å), mainly carbon atoms from the addend are detected. However, compound **4l** seems to show a very low degree of functionalization of about 0.9 at. %, which might indicate that the size of the molecules hinders the reaction process.

Table 1. Nitrogen to Carbon Ratio as Determined by XPS

compd	N-to-C ratio (at. %)	compd	N-to-C ratio (at. %)
4b	1.5	**4h**	1.5
4g	1.9	**4l**	0.9

Atomic Force Microscopy (AFM) and Transmission Electron Microscopy (TEM). Comparison of the AFM micrographs of the SWCNT starting material (Figure 8) and functionalized tubes (Figure 9) shows that even after functionalization the formation of bundles takes place. However, it appears that the average thickness of the bundles is reduced after functionalization as shown, for example, with the estimation of the height profile.[14] It cannot be decided whether the bundles of **4a**−**n** are present in solution or were subsequently formed during the drying process. These findings are corroborated by TEM. As demonstrated in Figure 10 the purity of the sample is increased due to the functionalization process. This can be deduced, for example, by the loss of amorphous carbon (black dots in Figure 10a) in the TEM micrograph of **4j** (Figure 10b).

Inspection of the TEM micrographs recorded at higher magnification reveals that the average thickness of the bundles is reduced considerably from about 30 nm in the SWCNT starting material to 10 nm in the functionalized tubes (Figure 11). Furthermore, it can be seen that there is a disorder in the bundles of functionalized tubes absent in the SWCNT starting material. This disorder within the bundles might be due to the intercalated addends causing partial disarray of the $\pi-\pi$-stacking interactions between the SWCNTs. This is only possible if the bundles are reestablished after the functionalization.

Solubility Properties. For the evaluation of the solubility properties the functionalsized SWCNTs **4a**−**n** were sonicated in a variety of solvents. Table 2 illustrates the influence of the nature of the nitrene addend on the solubility of the SWCNTs. In most cases, the presence of heteroatoms in the side chains as well as the presence of aromatic units increases the solubility of the SWCNTs. The highest solubilities were usually found in dimethyl sulfoxide (DMSO), 1,2-dichlorobenzene (ODCB), and 1,1,2,2-tetrachloroethane (TCE).

The results on the quantitative determination of the solubilities of **4a**−**n** are shown in Table 3. The solutions were prepared by sonicating the samples in DMSO. After a settling period of 24 h, the solution was decanted and the solvent evaporated. The weight of the residue was determined gravimetrically. This

(44) Carniato, S.; Dufour, G.; Luo, Y.; Agren, H. *Phys. Rev. B: Condens. Matter Mater. Phys.* **2002**, *66*, 045105/045101−045105/045112.
(45) Hüfner, S. *Photoelectron Spectroscopy*; Springer Verlag: Berlin, 1995.

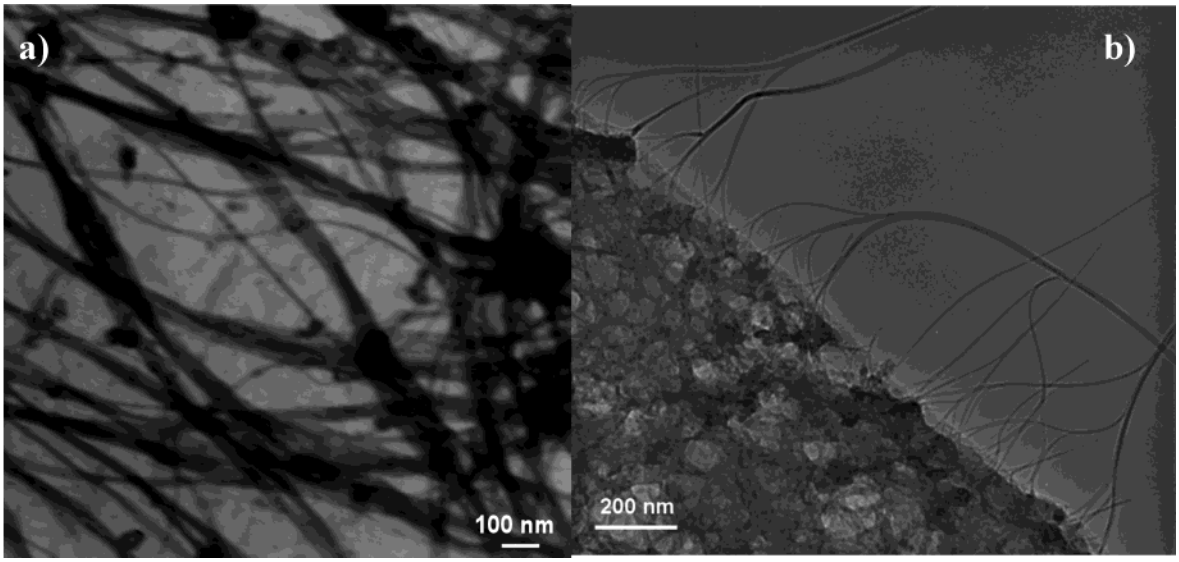

Figure 10. TEM image of SWCNT starting material (a) and **4j** (b) showing SWCNTs at a tear-off edge of the carbon film of the copper grid.

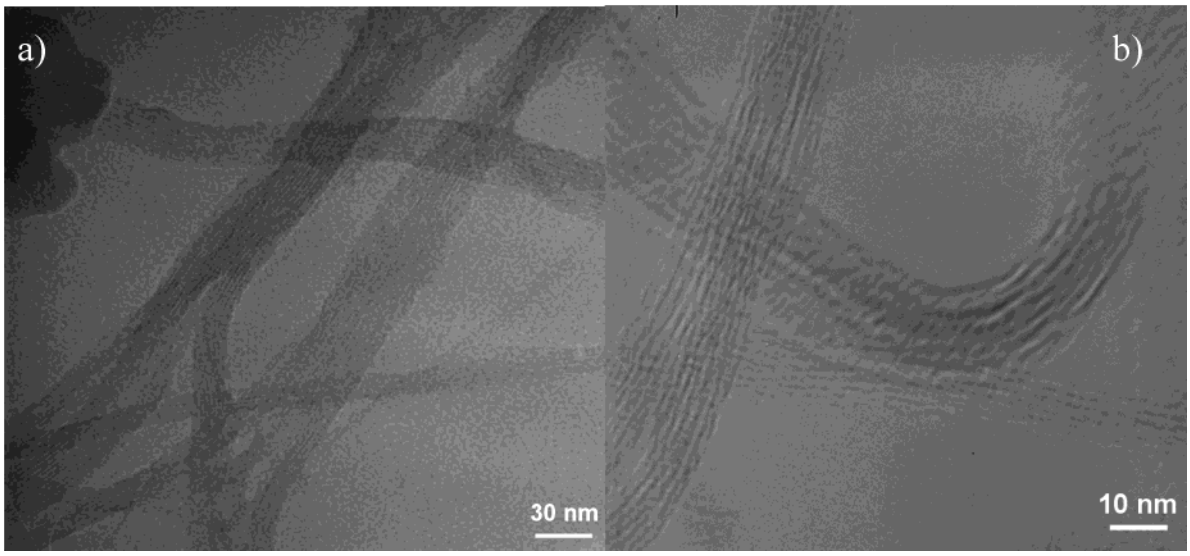

Figure 11. TEM image of SWCNT starting material and **4j** at higher resolution.

Table 2. Qualitative Solubility of the SWCNT Derivatives **4a**−**n** in a Variety of Solvents[a,b]

	a	b	c	d	e	f	g	h
4a	−	−	+	−	−	−	−	−
4b	0	0	+	0	−	−	−	0
4c	−	−	+	+	0	−	−	0
4d	−	−	+	−	−	−	−	0
4e	0	−	+	+	+	−	−	0
4f	−	−	+	+	−	−	−	0
4g	−	−	+	+	−	−	−	0
4h	+	−	+	+	0	0	−	0
4i	+	0	+	+	+	+	−	+
4j	+	−	+	+	−	0	−	0
4k	+	−	+	+	0	0	−	0
4l	0	−	+	+	0	−	−	−
4m	+	−	+	+	+	−	−	0
4n	+	+	+	+	+	0	−	0

[a] Solvents: (a) tetrachloroethane, (b) dichloromethane, (c) dimethyl sulfoxide (d) 1,2 dichlorobenzene, (e) dimethylformamide, (f) ethyl acetate, (g) carbon disulfide, (h) chloroform. [b] Solubilities: −, not soluble; 0, faintly colored solution; and +, dark black solution.

procedure was repeated five times to determine an average value for the solubility. The solubilities of **4b**, **4h**, **4k**, and **4l** were determined by ^{1}H NMR spectroscopy by comparison of the peak integration of the compound signals with those of an internal standard. With this method, we estimate an approximate value of the solubility of about 0.3−1.2 mg/mL for the functionalized SWCNTs. The solubility of the SWCNT starting material is equal to the solubility found by Tour and his group.[7] Interestingly, the expectation that **4l**, involving a second-generation dentritic addend, should have the highest solubility was not fulfilled; this might be due to the low degree of functionalization compared to the other compounds (Table 1).

The sidewall functionalization in general causes an increase of the solubility. The solubility of the most soluble derivatives **4j** and **4k** surpasses that of the SWCNT starting material by the factor of 10. We were unable to reproduce solubilities as high as 50 mg/mL reported for a variety of azomethine ylide adducts of SWCNTs.[15] The solubilities of about 1 mg/mL fit well the solubilities determined by other groups.[7,10,46] Furthermore, we detected a dramatic increase in the viscosity of the solutions with high SWCNT content. It should be kept in mind

(46) Pompeo, F.; Resasco, D. E. *Nano Lett.* **2002**, *2*, 369−373.

Table 3. Solubilities of the SWCNT Derivatives **4a**−**n** and SWCNT Starting Material (sm) in DMSO or TCE

compd	solvent	solubilty (mg/mL)	compd	solvent	solubilty (mg/mL)
sm	TCE	0.10	**4h**	TCE	0.50
4a[a]	DMSO		**4i**	DMSO	0.84
4b	DMSO	0.40	**4j**	DMSO	1.20
4c	DMSO	0.25	**4k**	TCE	1.20
4d	DMSO	0.16	**4l**	TCE	0.30
4e	DMSO	0.29	**4m**	DMSO	0.38
4f	DMSO	0.19	**4n**	DMSO	0.56
4g	DMSO	0.34			

[a] **4a** was not determined.

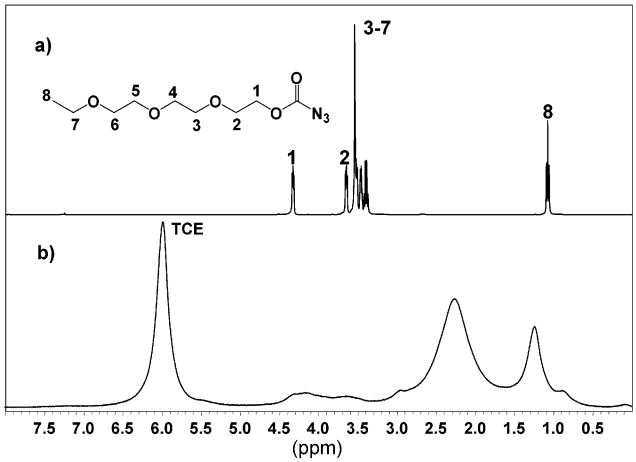

Figure 12. ^{1}H NMR spectra of (a) **3h** ($CDCl_3$) and (b) **4h** (TCE-d_2).

that the solubilities listed in Table 3 are not molar solubilities and therefore depend on the molecular weight of the addends.

^{1}H NMR Spectroscopy. Due to the increased solubility of the derivatives **4a**−**n**, we were able to carry out ^{1}H NMR spectroscopy in solution. Attempts to record ^{13}C NMR spectra failed. These investigations lead us to the following general observations: (1) All compounds give rise to individual and characteristic spectra. (2) The comparison of the spectra of **4a**−**n** with those of the azido- and chlorocarbonate precursors **2** and **3** shows analogies of the corresponding signal patterns. (3) Compared to the spectra of **2** and **3**, the corresponding resonances of **4** are considerably broadened. (4) The addend signals within **4** appear upfield shifted compared to those of **2** and **3**.

To illustrate these characteristics, we show three typical proton NMR spectra of functionalized SWCNTs in comparison to the precursor molecule in detail. All precursor molecules give rise to well-defined spectra with the expected chemical shifts and multiplicities. Figure 12 shows the proton NMR spectra of **3h** and the corresponding SWCNT derivative **4h**.

The spectrum of **4h** is dominated by two broad signals at $\delta = 2.3$ and 1.2, next to the solvent peak of TCE. We assign these signals to the protons 2−7 of the ether chain. The splitting up into two signals might be due to intercalation. We assume that the nanotube bundles partially exfoliate during the reaction and re-form after workup. As a consequence, a fraction of the addends is located within the interstitial channels of the bundles. This conclusion is also verified by the TEM images showing disorder within the SWCNT bundles (Figure 11). Protons of the addends inside the bundles are exposed to a stronger shielding caused by the surrounding π−system than the protons

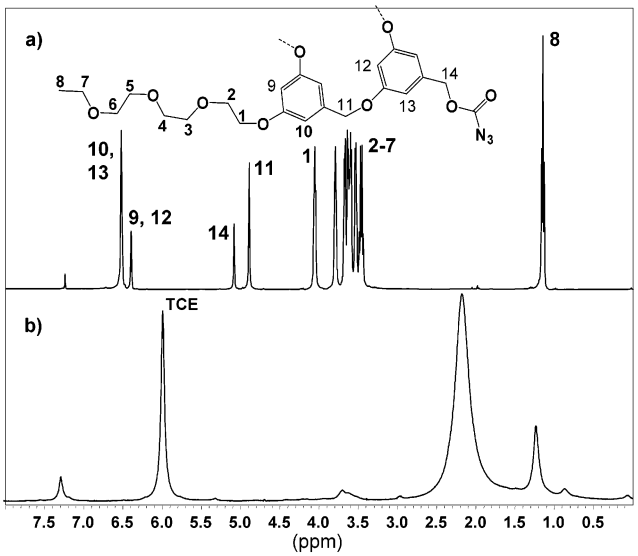

Figure 13. ^{1}H NMR spectra of (a) **3l** ($CDCl_3$) and (b) **4l** (TCE-d_2).

of addends located on the surface of the bundle. The less intensive but also broad signals at $\delta = 3.2-3.0$ and $\delta = 0.9-0.1$ are probably due to the protons 1 and 8. The reasons for the signal broadening are (a) the statistical distribution of the addends on the tube surface, (b) the fact the many different tubes that, for example, have different helicities are present, (c) that traces of metal catalyst required for the formation of the tubes are still present, and (d) that the sample was not completely solubilized. This is corroborated by the fact that also the solvent peak is considerably broadened.

In the case of the spectrum of **4l** (Figure 13b) the line broadening is less pronounced. The signal of the ether chains seems to undergo a similar splitting than those of **4h** (Figure 12). In the case of **4l**, it looks like that amount of addends intercalated within the bundles is smaller, because the relative intensity of the high-field signal is lower. This is expected, because the addends in **4l** are larger, preventing an efficient intercalation due to steric congestion.

More dramatic signal splitting is observed in the spectrum of **4n** (Figure 14). We assume that all the four signals at $\delta = 6.4$, 3.6, 1.7, and 1.1 correspond to the pyrenyl group. The different chemical shifts might be explained by different possible orientations of both external and intercalated pyrenyl addends. Due to the pronounced capability of the pyrenyl group to undergo $\pi-\pi$-stacking interactions with the neighboring SWCNT, face-to-edge and also face-to-face orientations are possible. Face-to-face orientations of both external and intercalated pyrenyl addends will lead to a more pronounced upfield shift, since the protons are located more closely to the π-systems of the tubes.

Optical Absorption Spectroscopy. With UV/Vis−nIR it is possible to detect three absorption bands caused by the electron transfers [$c_s^1 \leftrightarrow \nu_s^1$ at 1900 nm (0.66 eV), $c_s^2 \leftrightarrow \nu_s^2$ at 950 nm (1.31 eV), and $c_m^1 \leftrightarrow \nu_m^1$ at 650 nm (1.9 eV)][47] within the van Hove singularities.[48,49] In this study we looked at the two high-

(47) Odom, T. W.; Huang, J.-L.; Kim, P.; Lieber, C. M. *J. Phys. Chem. B* **2000**, *104*, 2794−2809.
(48) Chiang, I. W.; Brinson, B. E.; Smalley, R. E.; Margrave, J. L.; Hauge, R. H. *J. Phys. Chem. B* **2001**, *105*, 1157−1161.
(49) Ausman, K. D.; Piner, R.; Lourie, O.; Ruoff, R. S.; Korobov, M. *J. Phys. Chem. B* **2000**, *104*, 8911−8915.

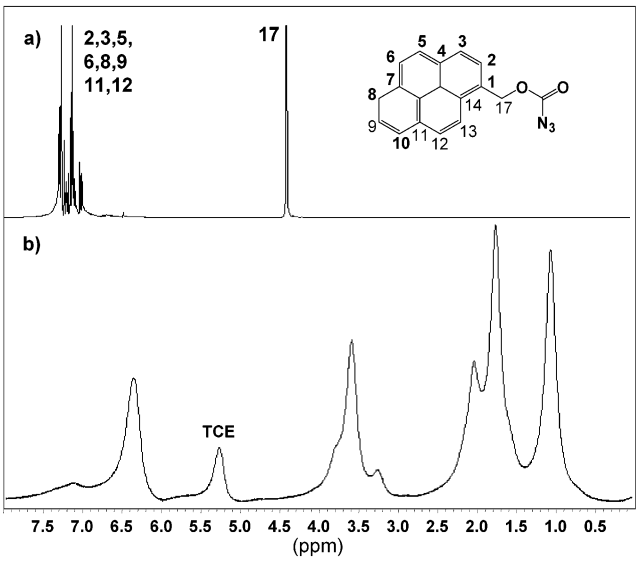

Figure 14. ^{1}H NMR spectra of (a) **3n** ($CDCl_3$) and (b) **4n** (TCE-d_2).

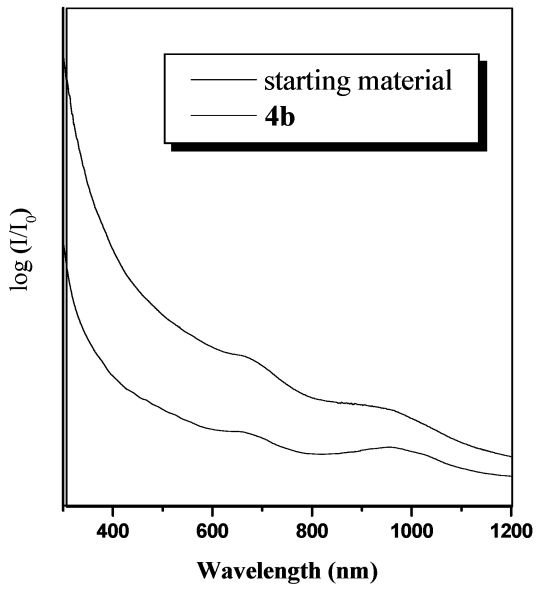

Figure 15. UV/Vis−nIR spectra of **4b** (bottom) and SWCNT starting material (top).

energy transitions at 950 and 650 nm in order to investigate whether the electronic properties of the SWCNTs remain unchanged or if they are disrupted due to the functionalization. All SWCNT derivatives still show the presence of the two bands with only minor changes in their shapes. Due to the fact that it is impossible to prepare a solution with a defined molar concentration of solublilized tubes, it cannot be determined whether the intensity of these van Hove bands has been decreased or not. This is demonstrated with Figure 15, which shows the spectra of **4b** (bottom line) and the SWCNT starting material (top line).

The comparison indicates that the degree of functionalization did not destroy the electronic properties of the SWCNTs. Detection of characteristic UV/Vis absorptions caused by the addends is another possibility to prove the chemical functionalization.

This is exemplified with the UV/Vis−nIR spectrum of **4n** (Figure 16), displaying the characteristic absorptions of the

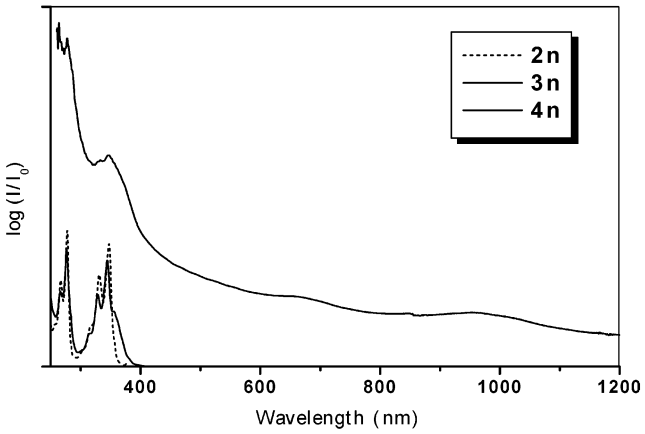

Figure 16. UV/Vis−nIR spectrum of **2n**, **3n**, and **4n**.

pyrenyl addends at 171 and 182 nm. These absorptions remain at the same position as those of the precursor molecules **2n** and **3n**.

Raman Spectroscopy. Raman spectroscopy is a widely used technique for probing the structure, diameter, and electronic properties of SWCNTs.[50−54] Raman scattering in SWCNTs is dominated by a resonant process, which is associated with optical transitions between 1D states in the electronic band structure. Raman spectra of SWCNTs contain three main features. The first one situated between ∼1530 and 1600 cm^{-1} is related to the C−C stretching tangential mode (TM) in graphite. The most intense band at ∼1590 cm^{-1} is referred to as the graphitic (G) band. The feature around 1300 cm^{-1} is termed the D band, due to it being related to scattering from defects present in the SWCNTs. The third region at around 180 cm^{-1} originates from the radial breathing mode (RBM), which is unique for SWCNTs.

As shown in Figure 17, the Raman spectrum of the SWCNT starting material exhibits a strong G band at 1597 cm^{-1} and two strong bands at 180 and 167 cm^{-1} in the RBM region. The weak D band at 1277 cm^{-1} is assigned to defects in the nanotube lattice, which include sp^3-hybridized carbon atoms.[55,56] The RBM is highly sensitive to the diameter of the tubes, being inversely proportional to the RBM position (ω_R). Many calculations have been developed to use this relationship for the estimation of tube diameters.[51,57,58] These include the recent calculation of Venkateswaran et al.:[59]

$$\omega_R = \frac{223.75\ \text{nm cm}^{-1}}{d\ (\text{nm})} + 14\ \text{cm}^{-1}$$

In this calculation, ω_R is the RBM frequency, d is the tube diameter, and 14 cm^{-1} represents a correction factor for the

(50) Kneipp, K.; Kneipp, H.; Corio, P.; Brown, S. D. M.; Shafer, K.; Motz, J.; Perelman, L. T.; Hanlon, E. B.; Marucci, A.; Dresselhaus, G.; Dresselhaus, M. S. *Phys. Rev. Lett.* **2000**, *84*, 3470−3473.
(51) Rao, A. M.; Bandow, S.; Richter, E.; Eklund, P. C. *Thin Solid Films* **1998**, *331*, 141.
(52) Kuzmany, H.; Burger, B.; Thess, A.; Smalley, R. E. *Carbon* **1998**, *36*, 709−712.
(53) Jorio, A.; Saito, R.; Hafner, J. H.; Lieber, C. M.; Hunter, M.; McClure, T.; Dresselhaus, G.; Dresselhaus, M. S. *Phys. Rev. Lett.* **2001**, *86*, 1118−1121.
(54) Duesberg, G. S.; Loa, I.; Burghard, M.; Syassen, K.; Roth, S. *Phys. Rev. Lett.* **2000**, *85*, 5436−5439.
(55) Bahr, J. L.; Tour, J. M. *Chem. Mater.* **2001**, *13*, 3823−3824.
(56) Mitchell, C. A.; Bahr, J. L.; Arepalli, S.; Tour, J. M.; Krishnamoorti, R. *Macromolecules* **2002**, *35*, 8825−8830.
(57) Wang, Y. F.; Cao, X. W.; Hu, S. F.; Liu, Y. Y.; Lan, G. X. *Chem. Phys. Lett.* **2001**, *336*, 47−52.
(58) Hulman, M.; Plank, W.; Kuzmany, H. *Phys. Rev. B: Condens. Matter Mater. Phys.* **2001**, *63*, 081406/081401−081406/081404.

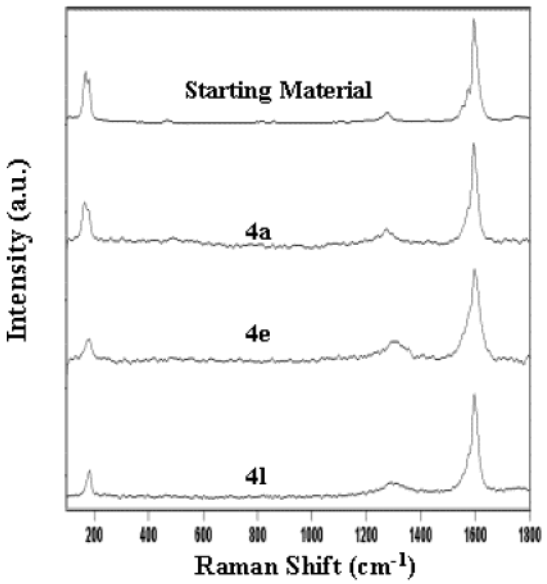

Figure 17. Raman spectra with 1064 nm excitation energy of SWCNT starting material, **4a**, **4e**, and **4l**.

Table 4. G Band Positions (ω_G), G Bandwidths (γ_G), D Band Positions (ω_G), I_D/I_G Ratios, and the RBM Positions (ω_R) in the Raman Spectrum (λ_{ex} = 1064 nm) of the SWCNT Starting Material (sm) and of the Functionalized SWCNTs (**4a**−**n**)

	ω_G (cm^{-1})	γ_G (cm^{-1})	ω_D (cm^{-1})	I_D/I_G	ω_{R1} (cm^{-1})	ω_{R2} (cm^{-1})
sm	1597	17.3	1277	0.08	180	167
4a	1596	20.4	1272	0.14	178	164
4b	1599	25.7	1304	0.15	183	174
4c	1598	22.7	1287	0.13	183	171
4d	1597	22.2	1287	0.15	181	170
4e	1599	29.0	1304	0.24	182	170
4f	1596	20.0	1281	0.20	182	170
4g	1599	25.0	1298	0.16	182	171
4i	1599	28.4	1281	0.13	183	170
4j	1598	29.1	1305	0.22	181	169
4k	1597	22.2	1285	0.10	182	170
4l	1598	24.4	1291	0.12	183	173
4m	1600	27.2	1301	0.23	180	167
4n	1600	27.7	1294	0.12	182	171

effect of the weak intertube interactions in a bundle. By applying this equation to the RBM bands of the SWCNT starting material, the average tube diameters were calculated to be in a range of 1.35−1.46 nm. However, it should be noted that the Raman studies performed here were at one fixed excitation energy (1064 nm). As Raman scattering in tubes is a resonant process, the position of the RBM is highly dependent on the excitation energy. Therefore, the use of additional energies is required to fully investigate the tube diameter distribution.

The G band positions (ω_G), G bandwidths (γ_G), D band positions (ω_D), I_D/I_G ratios, and the RBM positions (ω_R) of the functionalized-SWCNTs and the SWCNT starting material are shown in Table 4. First of all, it is important to know that no dramatic changes occurred in the Raman spectra. This observation correlates well with those from other groups performing Raman on functionalized SWCNTs.[13,60] However, the comparison of the Raman spectra shows some general trends for all the functionalized SWCNTs. The overall Raman scattering from the functionalized samples was greatly reduced compared to the starting unfunctionalized material. Their RBM intensities are reduced relative to the G band. The D band intensity increases for all samples; this is reflected in the increase in the I_D/I_G ratio values. There was an increase in the G bandwidth for all the samples, ranging from 2.7 to 11.8 cm^{-1}. The increase in the I_D/I_G ratio and G bandwidths are an indication of an increase in the defects in the nanotube lattice. This might, in part, be due to the introduction of covalently bound moieties to the nanotube framework, resulting in a conversion of a significant amount of sp^2-hybridized carbon to sp^3-hybridized carbon.

The Raman spectra of **4e** and **4l** (Figure 17) illustrate the variable increase of the D band, compared to the SWCNT starting material, for the different samples. It is expected that this is related to the different degrees of functionalization for each sample.

The increase in the D band is similar to the functionalized SWCNTs produced by other groups, if one takes into account that our degree of funtionalization is 0.9−1.9% (shown in Table 1) compared to 2.5−5%.[13,55]

Also, a slight upshift of the RBM band and a change in the relative intensity of the two bands was observed, for the majority of the samples. The intensity of the lower energy band was reduced compared to the higher energy band, which can be seen in the spectrum of **4e** (Figure 17). The decrease in the intensity of a RBM band may indicate a higher degree of functionalization for nanotubes of the corresponding diameter. However, here the larger diameter tubes are the most significantly affected. This was not what we expected, because the smaller diameter tubes have increased reactivity, due to their increased curvature strain, compared to the larger tubes.[61−63] These results lead to the possibility that the tube diameter distribution has been affected by the functionalization process.

The Raman spectra indicate that the diameter distribution has been changed by an increase of smaller tubes, relative to the larger tubes. If this is the case, it is likely that it is a result of the workup procedure, during which a suspension of the derivatized SWCNTs was separated by decantation from the insoluble contaminants that can include unmodified or barely modified SWCNTs. A shift in the RBM due to an electronic interaction could be eliminated due to the fact that there is an insignificant change in the G band positions.[60]

However, it is possible that the change in the RBM relative intensities is due to a different coupling of the electronic resonance enhanced spectra to the laser rather than a relative change in tube diameter populations in the functionalized samples. Changes in the size of the bundles, which were determined by TEM and AFM, are known to affect the RBM positions.[64−66] Therefore, it is also possible that the RBM shifts observed in this work are due to changes in the tube interactions and stacking behavior after the functionalization.

There is one major exception to these general observations. The ethyl-functionalized sample **4a** shows, instead of an upshift, a downshift of the RBM bands of 2−3 cm^{-1}. This may indicate

(59) Venkateswaran, U. D.; Rao, A. M.; Richter, E.; Menon, M.; Rinzler, A.; Smalley, R. E.; Eklund, P. C. *Phys. Rev. B: Condens. Matter Mater. Phys.* **1999**, *59*, 10928−10934.
(60) Kukovecz, A.; Kramberger, C.; Holzinger, M.; Kuzmany, H.; Schalko, J.; Mannsberger, M.; Hirsch, A. *J. Phys. Chem. B* **2002**, *106*, 6374−6380.
(61) Cai, L.; Bahr, J. L.; Yao, Y.; Tour, J. M. *Chem. Mater.*, ACS ASAP.
(62) Zhou, W.; Ooi, Y. H.; Russo, R.; Papanek, P.; Luzzi, D. E.; Fischer, J. E.; Bronikowski, M. J.; Willis, P. A.; Smalley, R. E. *Chem. Phys. Lett.* **2001**, *350*, 6−14.
(63) Chen, Z.; Thiel, W.; Hirsch, A. *ChemPhysChem* **2002**, in press.

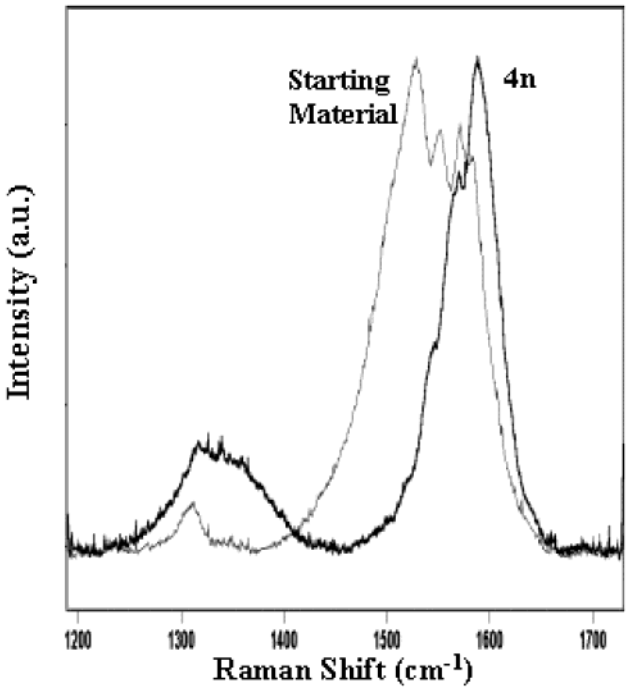

Figure 18. Raman spectra with 632 nm excitation energy of SWCNT starting material and **4n**.

a higher degree of functionalization for the nanotubes with smaller diameters. Once again, a shift due to an electronic interaction could be eliminated due to an insignificant change in the G band position. However, we could not fully explain the different behavior of **4a** compared to the other samples.

The Raman excitation energy of 1024 nm, used for recording the spectra in Figure 17, predominately probes semiconducting nanotubes. It is known that chemical treatments can exhibit different reactivities toward the tubes depending on their electronic structure.[67−69] Metallic tubes can be more reactive due to their smaller diameters, leading to larger curvature strain.[61−63] Also, it has been predicted that the curvature elastic energy in armchair (metallic) tubes is higher than in zigzag (semiconducting) tubes of similar diameters.[70]

Further, Raman experiments with an excitation energy of 632 nm enabled us to predominantly probe the metallic tubes. It was beyond the capabilities of the instrument, used for these measurements, to measure the RBM region. Therefore, further investigations of the tube diameter distribution were not possible.

The starting material TM displays the typical features expected for metallic tubes (Figure 18).[71,72] This includes the presence of a broad asymmetric band at ∼1540 cm^{-1} with a Breit−Wigner−Fano (BWF) profile. The BWF asymmetric shape is due to coupling between phonon scattering and electronic scattering in the metallic tubes.[69] After the functionalization (Figure 18b), it can be seen that the increase in the D band is greater for the metallic than the semiconducting tubes (Figure 17), which indicates that the degree of functionalization for the metallic tubes was greater than that of the semiconducting tubes. The functionalization has also had a much greater effect on the TM mode of the metallic tubes. First, the whole TM mode is significantly shifted upward, which indicates a charge transfer doping between the SWCNTs and the addend. There is also a strong suppression of the band at ∼1540 cm^{-1}. Overall, the TM becomes more symmetric and the most intense feature is now at ∼1590 cm^{-1}, which is more similar to the profile expected for semiconducting tubes.[71,72] The suppression of the band at 1540 cm^{-1} is expected to be due to functionalization affecting the phonon structure and coupling to isoenergetic electronic states above the shifted Fermi level.[69]

In general, the Raman experiments show that the reaction used here for the functionalization appears to preferentially interact with the metallic tubes. The small increase in the D band is probably due to the low degree of functionalization of the SWCNTs and indicates that the structure of the SWCNTs remains undestroyed.

Discussion and Outlook

These results constitute a fundamental basis in the science of the functionalization of single-walled carbon nanotubes. Here we present not only a large variety of functional groups attached to the SWCNTs but we also contribute a wide range of different characterization tools. Such functionalized carbon nanotubes involving improved solubility properties can be important for the development of new polymer composites with interesting mechanical and electrical properties.

A comprehensive characterization of all the synthesized compounds, including the chloro- and azidocarbonates, was carried out. The use of such a wide range of spectroscopic and microscopic methods and the comparison of the results give convincing proof that the reaction succeeded in the way we expected. It also demonstrates that only the combination a variety of techniques can give sufficient data for the characterization of the SWCNT derivatives.

A detailed insight into the changes in the electronic and chemical structure could be deduced from XPS spectroscopy.

The investigations, shown here, clearly demonstrate that XPS spectroscopy is a powerful tool for the study of functionalized SWCNTs. The range of XPS spectra recorded for this work show significant difference, which could be assigned to the modification due to the functionalization. Furthermore, this technique enabled us to demonstrate that the functional groups attached to the SWCNT sidewall retain their ability to complex metals.

Microscopic methods such as AFM and TEM are widely used for the characterization of derivatized SWCNTs. However, the information that could be obtained from these methods should not be overemphasized. For the compounds investigated here we were only able to observe a general overview on the sample to check the microscopic purity of the sample. So, we were able to see that the samples contain mainly SWCNTs and were nearly free of any impurities. We were also able to verify that

(64) Rols, S.; Righi, A.; Alvarez, L.; Anglaret, E.; Almairac, R.; Journet, C.; Bernier, P.; Sauvajol, J. L.; Benito, A. M.; Maser, W. K.; Munoz, E.; Martinez, M. T.; De la Fuente, G. F.; Girard, A.; Ameline, J. C. *Eur. Phys. J. B* **2000**, *18*, 201−205.
(65) Rao, A. M.; Chen, J.; Richter, E.; Schlecht, U.; Eklund, P. C.; Haddon, R. C.; Venkateswaran, U. D.; Kwon, Y. K.; Tomanek, D. *Phys. Rev. Lett.* **2001**, *86*, 3895−3898.
(66) Henrard, L.; Popov, V. N.; Rubio, A. *Phys. Rev. B: Condens. Matter Mater. Phys.* **2001**, *64*, 205403/205401−205403/205410.
(67) Lefrant, S.; Baltog, I.; Baibarac, M.; Mevellec, J. Y.; Chauvet, O. *Carbon* **2002**, *40*, 2201−2211.
(68) Yu, Z.; Brus, L. E. *J. Phys. Chem. B* **2001**, *105*, 6831−6837.
(69) Yu, Z.; Brus, L. *J. Phys. Chem. B* **2001**, *105*, 1123−1134.
(70) Zhang, S.; Zhao, S.; Lu, J.; Xia, M. *Phys. Rev.B: Condens. Matter Mater. Phys.* **2000**, *61*, 12693−12696.
(71) Alvarez, L.; Righi, A.; Guillard, T.; Rols, S.; Anglaret, E.; Laplaze, D.; Sauvajol, J. L. *Chem. Phys. Lett.* **2000**, *316*, 186−190.
(72) Sauvajol, J. L.; Anglaret, E.; Rols, S.; Alvarez, L. *Carbon* **2002**, *40*, 1697−1714.

the length of the tubes remained the same, which means that the SWCNTs were not significantly shortened due to the reaction procedure. Furthermore, a decrease in the diameter of the bundles was observed. The functionalization itself and organic byproducts were not detectable due to the limited resolution of the techniques.

The addition of (R)-alkoxycarbonylnitrenes to the nanotube sidewalls leads to an increased solubility of the SWCNTs. Our studies of the solubility properties of the modified SWCNTs have shown that a limit of solvated nanotubes can be expected which is independent of the weight of their addends. We additionally observed a continuous increase of viscosity of the solutions with concentrations between 0.4 and 1.2 mg/mL. These observations allow the conclusion that there might be a saturation concentration of about 1.5 mg/mL due to the high viscosity.

^{1}H NMR spectroscopy is a widely used tool for organic chemists, but in the field of the chemical functionalization of carbon nanotubes, some problems due to the inhomogenity and the lack of solubility of the samples arise. Nevertheless, we were able to record a range of different spectra of all compounds, which enabled us to study the effect of the SWCNT moiety on the addends.

UV/Vis−nIR spectroscopy mainly shows the presence of the expected signals of the SWCNTs. Nevertheless, **4n** shows that once a chromophor is present in the functional group the bands due to the chromophor appear in the spectrum. The comparison of the spectrum of the SWCNT derivative and the precursor compound shows that the bands of the chromophor are not significantly shifted. This is remarkable, due to the closeness of the tube to the chromophor, and does not agree with our expectations.

Raman spectroscopy is a technique frequently used for the characterization of carbon nanotubes. Here we show the Raman spectra of the functionalized tubes in comparison to the SWCNT starting material. The Raman spectra of the functionalized SWCNTs show an increase of the defects in the nanotube lattice after the functionalization procedure. This confirms our expectations due to the introduction of covalently bound moieties on the tube lattice. Furthermore a change in the RBM bands was detected; this leads us to the conclusion that the tube diameter distribution was possibly changed during the functionalization process.

Experimental Section

Chemical shifts are given in ppm relative to the appropriate solvent peak as standard reference. The resonance multiplicity is indicated as s (singlet), d (doublet), t (triplet), q (quartet), m (multiplet), or combinations of these. Broad resonances are designated with b. Compounds **3a**,**b** were synthesized according to a literature procedure.[34]

General Procedure for the Synthesis of Alkyl Chlorocarbonates. To a dry, nitrogen-purged 100 mL two-necked flask, equipped with gas inlet and pressure compensation, a 20% phosgene solution in toluene (2.0 equiv phosgene) was introduced at a temperature of 0 °C. (**Caution**: *phosgene is a very toxic compound and should be handled with care.*) To this solution, a solution of (1.0 equiv) of the alcohol (**1c**−**n**) in toluene was added slowly over about 20 min. After stirring for at least 1 h at this temperature, the solution was slowly warmed to room temperature and stirred overnight. The excess phosgene was removed by purging the solution with nitrogen for 2 h (the phosgene was absorbed in a KOH solution). The solvent was then removed in vacuo and the residual oil dried thoroughly in high vacuum and used as crude product for the next reaction step.

General Procedure for the Synthesis of Alkyl Aazidocarbonates. The crude product (**2c**−**n**) obtained in the previous reaction step was dissolved under N_2 in dry THF. Then 0.1 equiv of 18-crown-6 and 1.4 equiv of NaN_3 were added, and the resulting suspension was stirred for 4 d at room temperature. Solid residues were removed by filtration. The product solution was evaporated and the resulting oil was subjected to flash chromatographic separation (silica, 4 × 20 cm). The product fraction was evaporated and dried in high vacuum.

General Procedure for the Synthesis of Aziridino-SWCNTs. In a round-bottomed flask equipped with gas inlet, 20 mg of SWCNTs was dispersed in 200 mL of ODCB using an ultrasonic bath. The solution was degassed in high vacuum, purged with nitrogen, and preheated to 160 °C. A solution of 2 g of the azidocarbonate **3** in 5 mL of ODCB was added dropwise over a period of 20−30 min. The temperature was maintained at 160 °C for 45 min, after which the product mixture was cooled to room temperature. Workup proceeded by separating the suspension of the derivatized SWCNTs (**4a**−**n**) from the insoluble contaminants, such as unmodified or barely modified SWCNTs, by decantation. The supernatant was diluted with a solvent such as acetone to induce flocculation of all SWCNTs. Subsequent centrifugation and washing of the residue result in the removal of soluble byproducts. The remaining derivatized SWCNTs (**4a**−**n**) were decanted and dried under high vacuum.

1-Hexylheptyl Chlorocarbonate (2c). Quantities used: 10.67 mL of 20% phosgene solution in toluene (19.95 mmol of phosgene, 2 equiv) and 2 g (9.98 mmol) of **1c**. Formula: $C_{14}H_{27}ClO_2$. MW: 263. Colorless oil. Yield: 2.65 g (9.95 mmol, 99%). ^{1}H NMR ($CDCl_3$, 300 MHz): δ = 0.82 (t, 6H), 1.23 (d, 16H), 1.57 (m, 4H), 4.85 (m, 1H) ppm. ^{13}C NMR ($CDCl_3$, 75 MHz): δ = 12.3, 20.8, 20.9, 23.3, 23.9, 27.3, 27.7, 29.9, 30.1, 32.0, 35.8, 83.2, 148.6 ppm. IR (film): ν = 2930, 2859, 2320, 1776, 1466, 1379, 1261, 1165, 1119, 1014, 909, 840, 726, 690 cm^{-1}. MS (FAB, NBA): m/z = 263 [M^+], 226 [M^+ − Cl], 199 [M^+ − COCl].

2-Hexyldecyl Chlorocarbonate (2d). Quantities used: 18.24 mL of 20% phosgene solution in toluene (34.5 mmol of phosgene, 2 equiv) and 5 mL (17.2 mmol) of **1d**. Formula: $C_{17}H_{33}ClO_2$. MW: 305. Colorless oil. Yield: 5.3 g (17.1 mmol, 99%). ^{1}H NMR ($CDCl_3$, 300 MHz): δ = 0.83 (t, 6H), 1.20 (s, 24H), 1.65 (m, 1H), 4.15 (d, ^3J = 9.4 Hz) ppm. ^{13}C NMR ($CDCl_3$, 75 MHz): δ = 14.6, 23.2, 27.1, 29.5, 29.8, 30.0, 30.4, 30.9, 31.4, 32.3, 32.4, 37.8, 75.5, 151.2 ppm. IR (film): ν = 2927, 2856, 2304, 1780, 1465, 1378, 1270, 1159, 941, 808, 723, 689 cm^{-1}. MS (FAB, NBA): m/z = 304 [M^+], 269 [M^+ − Cl], 241 [M^+ − COCl], 225 [M^+ − OCOCl].

Cyclohexylmethyl Chlorocarbonate (2e). Quantities used: 17.38 mL of 20% phosgene solution in toluene (32.5 mmol of phosgene, 2 equiv) and 2 mL (16.25 mmol) of **1e**. Formula: $C_8H_{13}ClO_2$. MW: 177. Colorless oil. Yield: 2.54 g (14.4 mmol, 88.6%). ^{1}H NMR ($CDCl_3$, 300 MHz): δ = 0.91 (m, 2H), 1.18 (m, 4H), 1.65 (m, 5H), 4.06 (d, ^3J = 6.6 Hz, 2H) ppm. ^{13}C NMR ($CDCl_3$, 75 MHz): δ = 25.8, 26.3, 26.5, 29.3, 29.6, 37.3, 77.5, 151.1 ppm. IR (film): ν = 2930, 2856, 2673, 2308, 1779, 1451, 1371, 1286, 1238, 1142, 969, 941, 861, 835, 807, 778, 689, 623, 559 cm^{-1}. MS (EI): m/z = 113 [M^+ − COCl], 88 [M^{2+}].

2-Methoxyethyl Chlorocarbonate (2f). Quantities used: 54.18 mL of 20% phosgene solution in toluene (101.3 mmol of phosgene, 2 equiv) and 4 mL (50.7 mmol) of **1f**. Formula: $C_4H_7ClO_3$. MW: 139. Colorless oil. Yield: 3.51 g (25.3 mmol, 50%). ^{1}H NMR ($CDCl_3$, 300 MHz): δ = 3.34 (s, 3H), 3.65 (q, 2H), 4.38 (q, 2H) ppm. ^{13}C NMR ($CDCl_3$, 75 MHz): δ = 59.5, 69.9, 71.0, 151.2 ppm. IR (film): ν = 2953, 2895, 2328, 1995, 1779, 1451, 1405, 1364, 1246, 1160, 1025, 983, 867, 688 cm^{-1}. MS (EI): m/z = 123 [M^+ − CH_3], 88 [M^+ − CH_3 − Cl], 59 [M^+ − OCOCl], 47 [M^+ −CH_3 − OCOCl].

2-Methylthioethyl Chlorocarbonate (2g). Quantities used: 22.96 mL of 20% phosgene solution in toluene (43.4 mmol of phosgene, 2

equiv) and 2.05 mL (21.7 mmol) of **1g**. Formula: $C_4H_7ClO_2S$. MW: 155. Colorless oil. Yield: 2.5 g (16.2 mmol, 75%). ^{1}H NMR ($CDCl_3$, 300 MHz): $\delta = 2.10$ (s, 3H), 2.74 (t, $^3J = 6.95$ Hz, 2H), 4.37 (t, $^3J = 6.95$ Hz, 2H) ppm. ^{13}C NMR ($CDCl_3$, 75 MHz): $\delta = 14.5$, 30.6, 68.9, 149.4 ppm. IR (film): $\nu = 2966$, 2922, 2337, 1777, 1456, 1430, 1374, 1295, 1145, 1058, 999, 927, 825, 665 cm^{-1}. MS (EI): $m/z = 154$ [M^+], 91 [$M^+ - COCl$], 75 [$M^+ - OCOCl$], 61 [$M^+ - OCOCl - CH_3$].

2-[2-(2-Ethoxyethoxy)ethoxy]ethyl Chlorocarbonate, [G0]-OCOCl (2h). Quantities used: 40 mL of 20% phosgene solution in toluene (75.6 mmol of phosgene, 2 equiv) and 6.7 g (6.6 mL, 37 mmol) of **1h**. $C_9H_{17}ClO_5$. MW: 240. Colorless oil. Yield: not determined. ^{1}H NMR ($CDCl_3$, 400 MHz): $\delta = 4.19$ (t, $^3J = 4.9$ Hz, 2 H), 3.57 (t, $^3J = 4.7$ Hz, 2 H), 3.49 (s, 2 H), 3.48 (t, $^3J = 5.4$ Hz, 2 H), 3.43 (t, $^3J = 5.2$ Hz, 2 H), 3.41 (t, $^3J = 5.4$ Hz, 2 H), 3.36 (q, $^3J = 6.9$ Hz, 2 H), 1.04 (t, $^3J = 6.8$ Hz, 3 H) ppm. ^{13}C NMR ($CDCl_3$, 100.4 MHz): $\delta = 157.0$, 70.3, 70.2, 70.1, 69.4, 68.1, 67.0, 66.1, 14.7 ppm. IR (film): $\nu = 2974.1$, 2930.5, 2870.9, 1779.7, 1449.6, 1375.3, 1351.7, 1293.2, 1169.7, 1110.3, 1047.1, 946.6, 842.4, 688.2 cm^{-1}. MS (FAB, NBA): $m/z = 241$ [M^+H].

Poly(ethylene glycol)butyl Ether-oxy Chlorocarbonate (2i). Quantities used: 15.4 mL of 20% phosgene solution in toluene (28.8 mmol of phosgene, 2 equiv) and 3 mL (14.4 mmol) of **1i**. To complete the conversion of the alcohol, the reaction mixture was stirred for another 12 h at 50 °C. MW: ~269. Colorless oil. Yield: 4.17 g (14.3 mmol, 99%). ^{1}H NMR ($CDCl_3$, 300 MHz): $\delta = 0.85$ (t, $^3J = 7.3$ Hz, 3H), 1.30 (m, 2H), 1.50 (m, 2H), 3.39 (t, 2H), 3.56 (m), 3.71 (t, 2H), 4.39 (q, 2H) ppm. ^{13}C NMR ($CDCl_3$, 75 MHz): $\delta = 14.3$, 19.6, 32.1, 68.6, 70.4, 71.0, 71.1, 71.1, 71.2, 71.6, 71.7, 151.2 ppm. IR (film): $\nu = 2999$, 2952, 2871, 2246, 1968, 1779, 1456, 1353, 1296, 1250, 1168, 914, 842, 734, 688, 666 cm^{-1}. MS (FAB, NBA): $m/z = 401$ [M^+ (4 × glycol)], 269 [M^+ (3 × glycol)], 226 [M^+ (2 × glycol)].

18-Crown-[6]-methyl Chlorocarbonate (2j). Quantities used: 3.64 mL of 20% phosgene solution in toluene (6.8 mmol of phosgene, 2 equiv) and 1 g (3.4 mmol) of **1j**. To complete the conversion of the alcohol, the reaction mixture was stirred for another 12 h at 50 °C. Formula: $C_{14}H_{25}ClO_8$. MW: 357. Colorless oil. Yield: not determined. ^{1}H NMR ($CDCl_3$, 300 MHz): $\delta = 3.59$ (m, 20H), 3.65 (t, 2H), 3.72 (t, 1H), 4.39 (q, 2H) ppm. ^{13}C NMR ($CDCl_3$, 75 MHz): $\delta = 70.4$, 71.0, 71.1, 71.3, 71.4, 71.6, 71.9, 76.7, 151.1 ppm. IR (film): $\nu = 2869$, 2337, 1779, 1599, 1495, 1451, 1352, 1296, 1252, 1126, 994, 946, 839, 771, 689, 665 cm^{-1}. MS (FAB, NBA): $m/z = 357$ [M^+], 327 [$M^+ -$ Cl], 289 [$M^+ - COCl$], 275 [M^{+-} OCOCl].

3,5-Bis{2-[2-(2-ethoxyethoxy)ethoxy]ethoxy}benzyl Chlorocarbonate, [G1]-OCOCl (2k). Quantities used: 25 mL of 20% phosgene solution in toluene (47 mmol of phosgene, 2 equiv) and 12.0 g (23 mmol) of **1k**, [G1]-OH. Formula: $C_{24}H_{39}ClO_{10}$. MW: 522. Bright yellow oil. Yield: not determined. ^{1}H NMR ($CDCl_3$, 400 MHz): $\delta =$ 6.47 (s, 2 H), 6.45 (s, 1 H), 5.14 (s, 2 H), 4.05 (t, $^3J = 4.7$ Hz, 4 H), 3.79 (t, $^3J = 4.4$ Hz, 4 H), 3.67 (t, $^3J = 4.4$ Hz, 4 H), 3.64 (t, $^3J = 4.5$ Hz, 4 H), 3.60 (t, $^3J = 4.7$ Hz, 4 H), 3.53 (t, $^3J = 3.9$ Hz, 4 H), 3.47 (q, $^3J = 7.1$ Hz, 4 H, 7), 1.15 (t, $^3J = 7.1$ Hz, 6 H) ppm. ^{13}C NMR ($CDCl_3$, 100.4 MHz): $\delta = 160.0$, 150.4, 135.1, 107.2, 102.1, 73.0, 70.6, 70.5, 70.4, 69.6, 69.4, 67.4, 66.4, 14.9 ppm. IR (film): $\nu = 3092.6$, 2973.6, 2930.6, 2871.9, 1776.4, 1598.5, 1450.6, 1349.0, 1323.5, 1298.2, 1245.1, 1134.5, 1112.0, 1071.1, 1011.5, 949.2, 843.3, 686.6 cm^{-1}. MS (FAB, NBA): $m/z = 523$ [M^+H].

3,5-Bis(3,5-bis{2-[2-(2-ethoxyethoxy)ethoxy]ethoxy}benzyloxy)-benzyl Chlorocarbonate, [G2]-OCOCl (2l). Quantities used: 8 mL of 20% phosgene solution in toluene (15.6 mmol of phosgene, 2 equiv) and 8.2 g (7.8 mmol) of **1l**, [G2]-OH. Formula: $C_{54}H_{83}ClO_{20}$. MW: 1086. Yellow oil. Yield: not determined. ^{1}H NMR ($CDCl_3$, 400 MHz): $\delta = 6.54$ (s, 4 H), 6.54 (s, 2 H), 6.41 (s, 2 H), 6.41 (s, 1 H), 5.17 (s, 2 H), 4.91 (s, 4 H), 4.07 (t, $^3J = 4.9$ Hz, 8 H), 3.80 (t, $^3J = 4.8$ Hz, 8 H), 3.67 (t, $^3J = 4.5$ Hz, 8 H), 3.65 (t, $^3J = 4.8$ Hz, 8 H), 3.60 (t, $^3J = 4.9$ Hz, 8 H), 3.54 (t, $^3J = 4.9$ Hz, 8 H), 3.48 (q, $^3J = 7.1$ Hz, 8 H), 1.16 (t, $^3J = 7.1$ Hz, 12 H) ppm. ^{13}C NMR ($CDCl_3$, 100.4 MHz): $\delta = 160.3$, 160.01, 150.5, 138.6, 135.3, 107.5, 105.9, 102.6, 101.0, 73.0, 70.7, 70.6, 70.5, 69.9, 69.7, 69.5, 67.3, 66.5, 15.0 ppm. IR (film): $\nu = 3080.6$, 3040.9, 2972.1, 2930.3, 2870.9, 1776.7, 1596.5, 1449.6, 1348.7, 1322.5, 1297.2, 1246.1, 1136.8, 1106.5, 1068.1, 949.9, 842.3, 685.6 cm^{-1}. MS (FAB, NBA): $m/z = 1087$ [M^+H].

2-Phenylethyl Chlorocarbonate (2m). Quantities used: 26.86 mL of 20% phosgene solution in toluene (50.28 mmol of phosgene, 2 equiv) and 3 mL (25.14 mmol) of **1m**. Formula: $C_9H_9ClO_2$. MW: 185. Colorless oil. Yield: 4.65 g (25 mmol, 99%). ^{1}H NMR ($CDCl_3$, 300 MHz): $\delta = 2.94$ (t, $^3J = 7.1$ Hz, 2H), 4.41 (t, $^3J = 7.1$ Hz, 2H), 7.21 (m, 5H) ppm. ^{13}C NMR ($CDCl_3$, 75 MHz): $\delta = 34.4$, 71.9, 126.8, 128.5, 128.6, 135.9, 150.3 ppm. IR (film): $\nu = 3031$, 2964, 2283, 1951, 1776, 1605, 1498, 1456, 1375, 1146, 1086, 1031, 9734, 824, 749, 699, 682, 571 cm^{-1}. MS (EI): $m/z = 184$ [M^+], 122 [$M^+ - COCl$], 104 [$M^+ - OCOCl$], 91 [M^{2+}].

1-Pyrenylmethyl Chlorocarbonate (2n). Quantities used: 13.8 mL of 20% phosgene solution in toluene (25.8 mmol of phosgene, 2 equiv) and 3 g (12.9 mmol) of **1n**. Formula: $C_{18}H_{11}ClO_2$. MW: 295. Yellow solid. Yield: 3.16 g (10.7 mmol, 83%). ^{1}H NMR ($CDCl_3$, 300 MHz): $\delta =$ 5.15 (s, 2H), 8.12 (m, 9H) ppm. ^{13}C NMR ($CDCl_3$, 75 MHz): $\delta =$ 45.2, 123.2, 125.1, 126.1, 126.6, 127.7, 128.1, 128.4, 128.8, 129.6, 130.7, 131.1, 131.6, 132.4, 206.5 ppm. IR (KBr): $\nu =$ 3041, 1916, 1792, 1588, 1478, 1435, 1417, 1312, 1257, 1239, 1185, 1136, 1092, 1055, 962, 876, 844, 829, 756, 722, 702, 687, 668, 569 cm^{-1}. MS (FAB, NBA): $m/z = 231$ [$M^+ - COCl$], 215 [$M^+ - OCOCl$].

1-Hexylheptyl Azidocarbonate (3c). Quantities used: 0.91 g (14.0 mmol) of NaN_3 and 2.65 g (10 mmol) of **2c**. Formula: $C_{14}H_{27}N_3O_2$. MW: 269. Colorless oil. Yield: 2.24 g (8.3 mmol, 83%) ^{1}H NMR ($CDCl_3$, 300 MHz): $\delta =$ 0.81 (t, 6H), 1.21 (s, 16H), 1.45 (m, 4H), 4.76 (septet, 1H) ppm. ^{13}C NMR ($CDCl_3$, 75 MHz): $\delta =$ 14.0, 22.5, 25.1, 29.1, 31.7, 33.9, 80.2, 157.4 ppm. IR (film): $\nu =$ 2929, 2859, 2413, 2132, 2034, 1728, 1467, 1378, 1240, 1122, 933, 751, 725, 639, 563 cm^{-1}. MS (FAB, NBA): $m/z = 272$ [M^+], 256 [$M^+ - N$], 242 [$M^+ - N_2$], 194 [$M^+ - CON_3$].

2-Hexyldecyl Azidocarbonate (3d). Quantities used: 1.6 g (23.94 mmol) of NaN_3 and 5.2 g (17.1 mmol) **2d**. Formula: $C_{17}H_{33}N_3O_2$. MW: 311. Colorless oil. Yield: 4.81 g (15.5 mmol, 91%). ^{1}H NMR ($CDCl_3$, 300 MHz): $\delta =$ 0.81 (t, 6H), 1.06 (s, 24H), 1.61 (m, 1H), 4.03 (d, $^3J = 19.4$ Hz) ppm. ^{13}C NMR ($CDCl_3$, 75 MHz): $\delta =$ 14.4, 14.5, 23.0, 23.1, 27.0, 29.6, 29.9, 29.9, 30.3, 31.3, 31.3, 32.2, 32.3, 37.7, 71.8, 158.0 ppm. IR (film): $\nu =$ 2927, 2857, 2412, 2137, 1759, 1733, 1466, 1379, 1235, 1171, 987, 753, 723 cm^{-1}. MS (FAB, NBA): $m/z = 311$ [M^+], 284 [$M^+ - N_2$], 240 [$M^+ - OCON_3$].

Cyclohexylmethyl Azidocarbonate (3e). Quantities used: 1.31 g (20.16 mmol) of NaN_3 and 2.5 g (14.4 mmol) of **2e**. Formula: $C_8H_{13}N_3O_2$. MW: 183. Colorless oil. Yield: 2.27 g (12.4 mmol, 86%). ^{1}H NMR ($CDCl_3$, 300 MHz): $\delta =$ 0.93 (m, 2H), 1.17 (m, 4H), 1.65 (m, 5H), 3.95 (d, $^3J = 6.4$ Hz, 2H) ppm. ^{13}C NMR ($CDCl_3$, 75 MHz): $\delta =$ 24.4, 26.5, 28.2, 72.5, 156.5 ppm. IR (film): $\nu =$ 2928, 2855, 2673, 2408, 2135, 1731, 1451, 1388, 1352, 1233, 1114, 1074, 987, 891, 843, 752, 619, 563 cm^{-1}. MS (FAB, NBA): $m/z = 155$ [$M^+ -$ N_2], 112 [$M^+ - CON_3$], 96 [$M^+ - OCON_3$].

2-Methoxyethyl Azidocarbonate (3f). Quantities used: 0.77 g (11.8 mmol) of NaN_3 and 1.17 g (8.4 mmol) of **2f**. Formula: $C_4H_7N_3O_2$. MW: 145. Colorless oil. Yield: 1.06 g (7.3 mmol, 87%). ^{1}H NMR ($CDCl_3$, 300 MHz): $\delta = 3.32$ (s, 3H), 3.55 (q, 2H), 4.28 (q, 2H) ppm. ^{13}C NMR ($CDCl_3$, 75 MHz): $\delta =$ 57.3, 65.7, 68.2, 155.9 ppm. IR (film): $\nu =$ 2963, 2411, 2184, 2138, 1734, 1454, 1407, 1370, 1359, 1701, 1301, 1033, 954, 870, 844, 800, 751 cm^{-1}. MS (FAB, NBA): $m/z = 145$ [M^+].

2-Methylthioethyl Azidocarbonate (3g). Quantities used: 1.47 g (22.68 mmol) of NaN_3 and 2.5 g (16.2 mmol) of **2g**. Formula: $C_4H_7N_3O_2$. MW: 161. Colorless oil. Yield: 1.15 g (7.1 mmol, 44%). ^{1}H NMR ($CDCl_3$, 300 MHz): $\delta = 2.09$ (s, 3H), 2.70 (t, $^3J = 6.9$ Hz, 2H), 4.30 (t, $^3J = 6.9$ Hz, 2H) ppm. ^{13}C NMR ($CDCl_3$, 75 MHz): $\delta =$ 16.2, 32.5, 67.2, 157.8 ppm. IR (film): $\nu =$ 2922, 2362, 2341, 2137, 1731, 1478, 1380, 1233, 1116, 1013, 919, 862, 750, 687, 657 cm^{-1}.

MS (EI): $m/z = 149$ [$M^+ - N$], 134 [$M^+ - N_2$], 103 [$M^+ - N_3 - CH_3$], 74 [$M^+ - OCON_3$], 61 [$M^+ - OCON_3 - CH_3$].

2-[2-(2-Ethoxyethoxy)ethoxy]ethyl Azidocarbonate, [G0]-OCON$_3$ (3h). Quantities used: 2.8 g (44 mmol, 1.2 equiv) of NaN_3 and 9.3 g (37 mmol) of **2h**. Formula: $C_9H_{17}N_3O_5$. MW: 247. Colorless oil. Yield: 7.8 g (31 mmol, 71%). ^{1}H NMR ($CDCl_3$, 400 MHz): $\delta = 4.32$ (t, $^3J = 4.6$ Hz, 2 H), 3.64 (t, $^3J = 4.6$ Hz, 2 H), 3.53 (s, 2 H), 3.51 (t, $^3J = 2.7$ Hz, 2 H), 3.46 (t, $^3J = 3.5$ Hz, 2 H), 3.44 (t, $^3J = 4.1$ Hz, 2 H), 3.39 (q, $^3J = 7.0$ Hz, 2 H), 1.07 (t, $^3J = 7.1$ Hz, 3 H) ppm. ^{13}C NMR ($CDCl_3$, 100.4 MHz): $\delta = 150.3$, 70.5, 70.43, 70.40, 70.3, 69.4, 67.9, 66.2, 14.8 ppm. IR (film): $\nu = 2974.1$, 2928.5, 2870.9, 2183.2, 2137.9, 1732.7, 1454.6, 1374.3, 1351.7, 1237.2, 1169.7, 1113.3, 1033.1, 944.6, 844.4, 751.2 cm^{-1}. MS (FAB, NBA): $m/z = 248$ [M^+H].

Poly(ethylene glycol)butyl Ether-oxy Azidocarbonate (3i). Quantities used: 1.31 g (20.16 mmol) of NaN_3 and 4.17 g (14.4 mmol) of **2i**. MW: 275. Colorless oil. Yield: 3.39 g (12.3 mmol, 86%). ^{1}H NMR ($CDCl_3$, 300 MHz): $\delta = 0.84$ (t, $^3J = 7,3$ Hz, 3H), 1.29 (m, 2H), 1.49 (m, 2H), 3.39 (t, 2H), 3.55 (m), 3.66 (t, 2H), 4.29 (q, 2H) ppm. ^{13}C NMR ($CDCl_3$, 75 MHz): $\delta = 14.2$, 19.6, 32.0, 67.7, 68.7, 70.2, 70.4, 70.7, 70.9, 71.0, 71.5, 157.8 ppm. IR (film): $\nu = 2871$, 2185, 2138, 1733, 1478, 1354, 1240, 1116, 1035, 751 cm^{-1}. MS (FAB, NBA): $m/z = 320$ [M^+ (4 × glycol)], 276 [M^+ (3 × glycol)].

18-Crown-6-methyl Azidocarbonate (3j). Quantities used: 0.31 g (4.76 mmol) of NaN_3 and 1.21 g (3.4 mmol) of **2j**. Formula: $C_{14}H_{25}N_3O_8$. MW: 363. Colorless oil. Yield: 0.56 g (1.55 mmol, 46%). ^{1}H NMR ($CDCl_3$, 300 MHz): $\delta = 3.60$ (s, 20H), 3.67 (t, 2H), 4.28 (t, 3H) ppm. ^{13}C NMR ($CDCl_3$, 75 MHz): $\delta = 70.7$, 70.7, 70.8, 70.8, 70.9, 70.9, 71.0, 71.0, 71.1, 71.1, 71.2, 76.9, 157.8 ppm. IR (film): $\nu = 2876$, 2361, 2144, 2025, 1773, 1676, 1598, 1459, 1353, 1244, 1114, 1036, 992, 869, 800, 752 cm^{-1}. MS (FAB, NBA): $m/z = 360$ [M^+], 331 [$M^+ - N_2$], 317 [$M^+ - N_3$].

3,5-Bis{2-[2-(2-ethoxyethoxy)ethoxy]ethoxy}benzyl Chlorocarbonate, [G1]-OCON$_3$ (3k): Quantities used: 1.3 g (20 mmol, 1.2 equiv) of NaN_3 and 9.1 g (17 mmol) of **2k**. Formula: $C_{24}H_{39}N_3O_{10}$. MW: 529. Bright yellow oil. Yield: 7.6 g (14.5 mmol, 85%). ^{1}H NMR ($CDCl_3$, 400 MHz): $\delta = 6.44$ (s, 2 H), 6.40 (s, 1 H), 5.05 (s, 2 H), 4.03 (t, $^3J = 4.9$ Hz, 4 H), 3.77 (t, $^3J = 4.6$ Hz, 4 H), 3.64 (t, $^3J = 4.4$ Hz, 4 H), 3.61 (t, $^3J = 4.5$ Hz, 4 H), 3.58 (t, $^3J = 4.7$ Hz, 4 H), 3.51 (t, $^3J = 3.9$ Hz, 4 H), 3.45 (q, $^3J = 6.9$ Hz, 4 H), 1.13 (t, $^3J = 6.8$ Hz, 6 H) ppm. ^{13}C NMR (CDCl3, 100.4 MHz): $\delta = 159.9$, 157.2, 136.2, 106.8, 101.6, 70.6, 70.5, 70.4, 69.68, 69.62, 69.4, 67.3, 66.4, 14.9 ppm. IR (film): $\nu = 3088.6$, 2972.6, 2928.6, 2871.9, 2185.2, 2139.9, 1730.4, 1598.5, 1450.6, 1348.0, 1323.5, 1298.2, 1236.1, 1175.5, 1111.0, 1071.1, 1011.5, 953.2, 844.3, 753.1, 685.6 cm^{-1}. MS (FAB, NBA): $m/z = 529$ [M^+].

3,5-Bis(3,5-bis{2-[2-(2-ethoxyethoxy)ethoxy]ethoxy}benzyloxy)-benzyl Azidocarbonate, [G2]-OCON$_3$ (3l). Quantities used: 0.2 g (3.4 mmol, 1.2 equiv) of NaN_3 and 3.2 g (2.8 mmol) of **2l**. Formula: $C_{54}H_{83}N_3O_{20}$. MW: 1093. Yellow oil. Yield: 2.1 g (1.9 mmol, 67%). ^{1}H NMR ($CDCl_3$, 400 MHz): $\delta = 6.52$ (s, 4 H), 6.52 (s, 2 H), 6.39 (s, 2 H), 6.39 (s, 1 H), 5.08 (s, 2 H), 4.89 (s, 4 H), 4.06 (t, $^3J = 4.9$ Hz, 8 H), 3.79 (t, $^3J = 4.4$ Hz, 8 H), 3.66 (t, $^3J = 4.5$ Hz, 8 H), 3.64 (t, $^3J = 4.8$ Hz, 8 H), 3.59 (t, $^3J = 4.9$ Hz, 8 H), 3.53 (t, $^3J = 4.9$ Hz, 8 H), 3.46 (q, $^3J = 7.1$ Hz, 8 H), 1.15 (t, $^3J = 6.9$ Hz, 12 H) ppm. ^{13}C NMR ($CDCl_3$, 100.4 MHz): $\delta = 159.9$, 159.8, 157.2, 138.7, 136.4, 107.0, 105.8, 102.1, 101.0, 70.6, 70.5, 70.4, 69.8, 69.7, 69.6, 69.4, 67.3, 66.4, 15.0 ppm. IR (film): $\nu = 3078.6$, 3045.9, 2975.1, 2928.3, 2865.9, 2173.2, 2127.9, 1731.7, 1596.5, 1449.6, 1348.7, 1322.5, 1297.2, 1237.1, 1136.8, 1114.5, 1069.1, 951.9, 843.3, 683.6 cm^{-1}. MS (FAB, NBA): $m/z = 1094$ [M^+H]. UV/Vis ($CHCl_3$): λ_{max} (ϵ) = 281.0 nm (2600 L mol^{-1}cm^{-1}).

2-Phenylethyl Azidocarbonate (3m). Quantities used: 2.29 g (35.2 mmol) of NaN_3 and 4.65 g (25.8 mmol) of **2m**. Formula: $C_9H_9N_3O_2$. MW: 191. Colorless oil. Yield: 4.56 g (23.8 mmol, 92%). ^{1}H NMR ($CDCl_3$, 300 MHz): $\delta = 2.90$ (t, $^3J = 7.1$ Hz, 2H), 4.31 (t, $^3J = 7.1$ Hz, 2H), 7.18 (m, 5H) ppm. ^{13}C NMR ($CDCl_3$, 75 MHz): $\delta = 36.6$, 70.5, 128.6, 130.3, 130.6, 138.5, 159.1 ppm. IR (film): $\nu = 3030$, 2963, 2405, 2137, 1952, 1875, 1730, 1605, 1498, 1456, 1384, 1237, 1087, 1051, 1032, 984, 945, 929, 846, 749, 699 cm^{-1}. MS (EI): $m/z = 163$ [$M^+ - N_2$], 149 [$M^+ - N_3$], 120 [$M^+ - CON_3$], 104 [$M^+ - OCON_3$].

1-Pyrenylmethyl Azidocarbonate (3n). Quantities used: 0.98 g (15.0 mmol) of NaN_3 and 3.16 g (10.7 mmol) of **2n**. Formula: $C_{18}H_{11}N_3O_2$. MW: 301. Yellow solid. Yield: 2.38 g (7.9 mmol, 74%). ^{1}H NMR ($CDCl_3$, 300 MHz): $\delta = 4.73$ (s, 2H), 7.82 (m, 9H) ppm. ^{13}C NMR ($CDCl_3$, 75 MHz): $\delta = 53.4$, 123.0, 125.0, 125.3, 125.9, 126.0, 126.5, 127.3, 127.7, 127.8, 127.9, 128.2, 128.6, 128.7, 129.5, 131.1, 131.6, 132.1, 207.7 ppm. IR (film): $\nu = 3039$, 2964, 2361, 2343, 2097, 1719, 1603, 1491, 1458, 1417, 1262, 1182, 1097, 893, 841, 804, 756, 705, 680, 669 cm^{-1}. MS (FAB, NBA): $m/z = 288$ [$M^+ - N$], 273 [$M^+ - N_2$], 257 [$M^+ - N_3$], 215 [$M^+ - OCON_3$].

Ethyl Azidocarbonate, EtOC−N$_3$ (3a). Formula: $C_3H_5N_3O_2$. MW: 104. Colorless oil. Yield: 6.4 g (61 mmol, 61%). ^{1}H NMR ($CDCl_3$, 400 MHz): $\delta = 4.20$ (q, $^3J = 7.9$ Hz, 2 H), 1.26 (t, $^3J = 7.3$ Hz, 3H) ppm. ^{13}C NMR ($CDCl_3$, 100.4 MHz): $\delta = 157.5$, 64.7, 14.1 ppm. IR (film): $\nu = 2987.8$, 2928.5, 2182.4, 2134.4, 1757.8, 1731.5, 1468.6, 1369.3, 1235.9, 1096.2, 1024.1 943.6, 877.4, 752.2 cm^{-1}.

***tert*-Butyl Azidocarbonate, BOC−N$_3$ (3b).** Formula: $C_5H_9N_3O_2$. MW: 143. Colorless oil. Yield: 11.2 g (78 mmol, 78%). ^{1}H NMR ($CDCl_3$, 400 MHz): $\delta = 1.58$ (s, 9 H) ppm. ^{13}C NMR ($CDCl_3$, 100.4 MHz): $\delta = 155.8$, 84.6, 27.7 ppm. IR (film): $\nu = 2984.1$, 2931.5, 2180.4, 2132.4, 1731.8, 1459.6, 1396.3, 1372.0, 1247.4, 1148.3, 1018.2, 946.6, 858.4, 754.2 cm^{-1}.

Ethyloxycarbonylaziridino-SWCNTs, EtOC-SWCNTs (4a). ^{1}H NMR (TCE-d_2, 400 MHz): $\delta = 3.83$, 1.79, 1.18, 0.08 ppm. Vis−nIR (TCE): $\lambda_{max} = 1.22$, 1.80 eV. Raman spectroscopy (excitation energy 1064 nm): 1596, 178, 164 cm^{-1}.

***tert*-Butyloxycarbonylaziridino-SWCNTs, BOC-SWCNTs (4b).** ^{1}H NMR (DMSO-d_6, 400 MHz): $\delta = 1.20$ ppm. Vis−nIR (solid film): $\lambda_{max} = 0.68$, 1.29, 1.83, 5 eV. FTIR (solid film): $\nu = 2852$, 2923, 2952, 1741, 1461 cm^{-1}. Raman spectroscopy (excitation energy 1064 nm): 1599, 183, 173 cm^{-1}.

1-Hexylheptoxycarbonylaziridino-SWCNTs (4c). ^{1}H NMR (ODCB-d_4, 300 MHz): $\delta = 0.95$, 1.34, 1.63 ppm. UV/Vis (DMSO): λ_{max} (ϵ) = 944, 655 nm. Raman spectroscopy (excitation energy 1064 nm): 1598, 183, 171 cm^{-1}.

2-Hexyldecoxycarbonylaziridino-SWCNTs (4d). ^{1}H NMR (DMSO-d_6, 300 MHz): $\delta = 1.03$, 1.23, 1.45 ppm. UV/Vis (DMSO): λ_{max} (ϵ) = 961, 662 nm. Raman spectroscopy (excitation energy 1064 nm): 1597, 181, 170 cm^{-1}.

Cyclohexylmethoxycarbonylaziridino-SWCNTs (4e). ^{1}H NMR (ODCB-d_4, 300 MHz): $\delta = 1.00$, 1.28, 1.44, 4.08 ppm. UV/Vis (DMSO): λ_{max} (ϵ) = 953, 661 nm. Raman spectroscopy (excitation energy 1064 nm): 1599, 182, 170 cm^{-1}.

2-Methoxyethoxycarbonylaziridino-SWCNTs (4f). ^{1}H NMR (ODCB-d_4, 300 MHz): $\delta = 1.56$, 2.17, 2.81 ppm. UV/Vis (DMSO): λ_{max} (ϵ) = 975, 661 nm. Raman spectroscopy (excitation energy 1064 nm): 1596, 182, 170 cm^{-1}.

2-Methylthioethoxycarbonylaziridino-SWCNTs (4g). ^{1}H NMR (ODCB-d_4, 300 MHz): δ =1.28, 2.10, 4.07 ppm. UV/Vis (DMSO): λ_{max} (ϵ) = 972, 663 nm. Raman spectroscopy (excitation energy 1064 nm): 1599, 182, 171 cm^{-1}.

1-(1-{2-[2-(2-Ethoxyethoxy)ethoxy]ethoxy}carbonylaziridino-SWCNTs (4h). ^{1}H NMR (TCE-d_2, 400 MHz): $\delta = 4.16$, 3.65, 2.26, 1.23, 1.18, 0.88, 0.08 ppm. Vis−nIR (TCE): $\lambda_{max} = 1.25$, 1.79 eV.

Poly(ethylene glycol)butyl Ether-oxy Carbonylaziridino-SWCNTs (4i). ^{1}H NMR ($CDCl_3$, 300 MHz): $\delta = 0.79$, 1.18, 1.30, 1.47, 2.84, 3.33, 3.67 ppm. UV/Vis (DMSO): λ_{max} (ϵ) = 965, 664 nm. Raman spectroscopy (excitation energy 1064 nm): 1599, 183, 170 cm^{-1}.

18-Crown-6-methoxycarbonylaziridino-SWCNTs (4j): ^{1}H NMR (TCE-d_2, 300 MHz): $\delta = 1.10$, 3.94 ppm. UV/Vis (DMSO): λ_{max} (ϵ) = 961, 665 nm. Raman spectroscopy (excitation energy 1064 nm): 1598, 181, 169 cm^{-1}.

3,5-Bis{2-[2-(2-ethoxyethoxy)ethoxy]ethoxy}benzyloxycarbonylaziridino SWCNTs, G1-SWCNTs (4k): ^{1}H NMR (TCE-d_2, 400 MHz): δ = 3.62, 2.12, 0.9 ppm. Vis−nIR (TCE): λ_{max} = 1.25, 1.79 eV. Raman spectroscopy (excitation energy 1064 nm): 1597, 182, 170 cm^{-1}.

3,5-Bis(3,5-bis{2-[2-(2-ethoxyethoxy)ethoxy]ethoxy}benzyl)benzyloxycarbonylaziridino SWCNTs, G2-SWCNTs (4l): ^{1}H NMR (TCE-d_2, 400 MHz): δ = 7.27, 3.69, 2.17, 0.86, 0.07 ppm. Vis−nIR (TCE): λ_{max} = 1.25, 1.79 eV. Raman spectroscopy (excitation energy 1064 nm): 1598, 183, 173 cm^{-1}.

2-Phenylethoxycarbonylaziridino-SWCNTs (4m): UV/Vis (DMSO): λ_{max} (ϵ) = 969, 665 nm. Raman spectroscopy (excitation energy 1064 nm): 1600, 180, 167 cm^{-1}.

1-Pyrenylmethoxycarbonylaziridino-SWCNTs (4n): ^{1}H NMR (TCE-d_2, 300 MHz): δ = 4.26, 7.17 ppm. UV/Vis (DMSO): λ_{max} (ϵ) = 959, 661 nm. Raman spectroscopy (excitation energy 1064 nm): 1600, 182, 171 cm^{-1}.

Cd^{2+} [18-Crown-6-methoxycarbonylaziridino-SWCNTs] (5j). In a 50 mL round-bottomed flask, 3 mg of **4j** was dispersed in 5 mL of 2-propanol. To the suspension was added 100 mg of $CdSO_4$ and the mixture was sonicated for another hour. The mixture was washed 10 times with 2-propanol and filtered using a cellulose nitrate pore filter (0.2μm) forming a "bucky paper" that was washed with distilled water.

3,5-Bis(3,5-bis{2-[2-(2-ethoxyethoxy)ethoxy]ethoxy}benzyl)benzyloxycarbonylaziridino-SWCNTs−Cu(II) Complex, Cu−[G1]-SWCNTs (5k). In a 50 mL round-bottomed flask, 5 mg of **4k** was dispersed in an aqueous $CuSO_4$ solution (c = 5.9 10^{-2} mol/L) by sonication overnight. The mixture was filtered using a cellulose nitrate pore filter (0.2μm) forming a "bucky paper" that was washed with distilled water. Vis−nIR (DMSO): λ_{max} = 1.22, 1.79 eV.

Acknowledgment. This work was carried out with support from the European Union (HPRNT-CT-1999-00011-FUNCARS).

Supporting Information Available: XPS survey scan of **5j** and the XPS N 1s and Cd 3d spectrum of **5j**. This material is available free of charge via the Internet at http://pubs.acs.org.

JA029931W